

Dependence of the critical temperature and disorder in holographic superconductors on superfluid density

Zhenguo Wang^{a*}, Xian-Hui Ge^{a,b†}, and Shuta Ishigaki^{a‡}

^a*Department of Physics, Shanghai University, Shanghai, 200444, China*

^b*Shanghai Key Laboratory of High Temperature Superconductors, Shanghai University, Shanghai, 200444, China*

Abstract

Recent experiments strongly indicate deep connections between transports of strange metal and high T_c superconductors. For example, the dependence of the zero-temperature phase stiffness on the critical superconducting temperature is generally linear, which is incompatible with the standard Bardeen-Cooper-Schrieffer description. We develop an analytical method for AC conductivity calculation and explore the scaling relations among superconducting critical temperature, superfluid density, and momentum dissipation strength for the Gubser-Rocha model with extensions in the probe limit. In the normal phase, we show that the critical temperature is proportional to the momentum dissipation strength in a certain parameter range, which is universal in holographic models. In the superconducting phase, studying the AC conductivity analytically and numerically, we find linear dependence of zero-temperature superfluid density (phase stiffness) on the critical superconducting temperature, which is consistent with recent experiments of high T_c superconductors. These results further underpin the deep connections between strange metal and high T_c superconductors.

*wang_zg@shu.edu.cn

†gexh@shu.edu.cn (corresponding author)

‡shutaishigaki@shu.edu.cn

Contents

1	Introduction	2
2	Setup	4
3	Scaling relation between T_c and k	7
3.1	Phase boundaries	7
3.2	Condensation	11
4	Linear dependence of T_c on the superfluid density	11
4.1	AC conductivity in the normal phase	13
4.2	Numerical results for the AC conductivity in the SC phase	14
4.3	Approximation for the AC conductivity in the SC phase	17
5	Discussion and Conclusion	19
	Appendix A Checking the correctness of the probe limit	21
	Appendix B Low temperature approximation for the AC conductivity in the SC phase	23

1 Introduction

Superconductivity is a very significant discovery in physics in the early part of the 20th century. Since its ascertainment, overwhelming experimental and theoretical research has been done on superconductivity, one of the most striking is BCS theory [1]. This theory assumes that the fundamental characteristics of superconductivity are caused by Cooper's pair correlation. As experiments progressed, high-temperature oxide superconductors [2–5] and iron-based superconductors [6–9] were found. The description of these superconductors is beyond the scope of BCS theory. Recently, a series of groundbreaking experimental findings have emerged that demonstrate how the superfluid density increasingly manifests a linear relationship with temperature as temperatures escalate [10–12]. This phenomenon departs from the conventional expectations set by the Bardeen-Cooper-Schrieffer (BCS) theory, thereby shedding light on potentially novel facets of high-temperature superconductivity and its fundamental physics. There are a lot of interests and challenges in studying the critical temperature T_c related to the superfluid density n_s . Some experimental papers [13–15] elucidate that T_c seems to be principally controlled by the superfluid density. More remarkably, the superfluid density displays a strong linear temperature dependence within a certain temperature range.

In this paper, we explore the universal properties of the superconductors, e.g., scaling relations, by using the AdS/CFT correspondence in a specific holographic model. The AdS/CFT correspondence [16–18], also known as holography or gauge/gravity duality, is a framework for tracing the behavior of strongly-coupled quantum systems in terms of a higher dimensional gravity theory. It can be a very powerful and fascinating tool to tackle strongly interacting systems by studying gravitational models. In particular, holographic techniques have been widely applied for studying condensed matter physics [19–22].

The kind of model called holographic superconductors is still an attractive topic of theoretical research. They have the potential to provide new insights into the nature of superconducting materials and could lead to the development of new technologies based on superconductivity. Based on the AdS/CFT correspondence, the first minimal bottom-up construction had been implemented

by Hartnoll, Herzog, and Horowitz [23]. In Ref. [23], the authors considered the charged complex scalar and the Maxwell field in the Schwarzschild-AdS₄ (SAdS₄) spacetime. Although this is a simple model, it can reproduce the typical behavior of the superconductor successfully. The calculation done in [23] was the so-called probe limit, ignoring the backreactions to the gravity sector from the matter sector. In [24], the authors considered the Einstein-Maxwell theory with the complex scalar and found that the probe-limit calculation corresponds to the infinite charge case with appropriate scaling. In any case, the complete analysis of the superconducting phase requires numerical computations. Meanwhile, some analytic properties of the holographic superconductor in the superconducting phase have been studied [25–27]. Since the complete analysis requires numerical computations, they provided some approximate formulas. From then on [23, 24], many papers have appeared that attempt to apply this useful idea to investigate superconductors in different setups [28–36].

Recently, it has been recognized that the strange metallic behavior is universal in superconductors like the high- T_c cuprates. The strange metal is often described by its linear- T dependence of the resistivity [37–39]. In holographic studies, the Gubser-Rocha model [40] is known as one of the candidates describing the strange metallic behavior of the superconductors. This model is an Einstein-Maxwell-dilaton theory, and axion fields are often introduced to break the translational invariance [41, 42]. The original model is consistent with the specific truncation of the 11-dimensional supergravity. This model has been widely utilized for studying the holographic version of the high- T_c cuprates superconductors. On the other hand, we notably advance the analytical framework for studying holographic superconductors by developing novel approximate methods to explore key analytic properties within the context of the Gubser-Rocha model. Despite the prevalent reliance on numerical computations in previous studies, akin to those conducted in the foundational holographic superconductor paradigm, we focus our efforts here on investigating analytically significant aspects such as the critical temperature and alternating current (AC) conductivity.

The primary objective of this paper is to investigate the scaling relationships connecting the superconducting critical temperature, the superfluid density, and the momentum-dissipation strength within the framework of the holographic superconductor model derived from the Gubser-Rocha model. Moreover, a significant part of our study involves comparing these theoretically deduced relations with empirical results obtained in experimental settings. First, we study the critical temperature by finding the onset of the charged-scalar instability. Taking advantage of the Sturm-Liouville method, we investigate how the momentum-dissipation strength affects the critical temperature. The results obtained by numerical and approximate methods are in good agreement with each other. Using the approximate formula, we find the scaling relation between the critical temperature and the strength of the momentum dissipation. Subsequently, we delve into the study of the AC conductivity in the superconducting state. To extract the superfluid density, we meticulously analyze the AC conductivity data and proceed to examine the correlation between the zero-temperature superfluid density and the critical temperature. Consequently, our findings reveal a linear scaling relationship between these parameters in a particular scenario, which strikingly aligns with recent experimental outcomes observed in copper oxides [15]. Finally, we develop and scrutinize an analytical approximate formula for the AC conductivity specifically tailored for the superconducting phase.

In brief, this paper is driven by three core motivations and objectives:

Unveiling Universal Behavior: The first pivotal objective centers around the exploration of the universal characteristics of the superfluid density within our holographic superconductor model. The main findings are encapsulated in Fig. 8 and Eq. (48), which represent the cornerstone results of this study. To substantiate this relationship across the entire temperature range within the superconducting phase, it necessitates the meticulous computation of several fundamental superconductor properties within our theoretical framework.

Implementing Probe-Limit Calculations: Throughout the paper, we effectively achieve the secondary aim through demonstrating the probe-limit calculation within our holographic model grounded on the Gubser-Rocha model. This endeavor not only serves as a methodological achievement but also holds significant physical implications for developing more realistic models of high-temperature superconductors. As an example, the extension to d-wave superconductors can be readily explored by substituting the appropriate matter sector. Thus, our research constitutes a foundational step towards considering such extensions.

Analyzing Analytic Results: For the third goal, equations (32) and (59) correspondingly highlight the analytic outcomes of our study. Notably, the linear relation depicted in equation (32) appears to exhibit universality across various holographic models incorporating momentum-dissipation strength. Despite securing only a limited number of analytical results, this investigation underscores the challenges and limitations inherent to analytical studies within our specific model, thereby contributing to a deeper understanding of its complexity and scope.

The organization of this paper is as follows. The holographic setup of our model is given in section 2. We investigate the critical temperature of the superconducting phase in section 3. In section 4, we turn to study the conductivity, and consider an analytic approximation for the AC conductivity in the superconducting phase. We provide conclusion and discussion in section 5. In Appendix A, we demonstrate how the profile of the critical temperature with general q from the full analysis with backreactions agrees with the probe limit results in a large q limit. In Appendix B, we show another approximate formula for the AC conductivity.

2 Setup

In this study, we employ the Gubser-Rocha model [40] extended with the linear axions and the charged scalar, for studying the superconducting nature [43–46]. The action of our model is given by [45, 46]

$$S = \int d^4x \sqrt{-g} (\mathcal{L}_g + \mathcal{L}_m), \quad (1a)$$

$$\mathcal{L}_g = R - \frac{1}{2}(\partial\phi)^2 + 6 \cosh \frac{\phi}{\sqrt{3}} - \frac{1}{2} \sum (\partial\psi_I)^2, \quad (1b)$$

$$\mathcal{L}_m = -\frac{1}{4} e^{\frac{\phi}{\sqrt{3}}} F^2 - |D\Phi|^2 - B(\phi)|\Phi|^2. \quad (1c)$$

The action consists of two components, \mathcal{L}_g representing the Lagrangian of fields involving the gravity and \mathcal{L}_m representing the Lagrangian of matter fields. The model involves gravity fields $g_{\mu\nu}$, a dilaton ϕ , axions ψ_I , $U(1)$ gauge fields and a complex scalar field Φ . It was shown that the presence of the dilaton field can realize the vanishing entropy at zero temperature [47]. The axions are originally introduced to break the translational invariance explicitly in the full analysis with backreactions [43]. $F_{\mu\nu} = \partial_\mu A_\nu - \partial_\nu A_\mu$ is the field strength of the $U(1)$ gauge field. The covariant derivative D is defined by $D_\mu := \nabla_\mu - iqA_\mu$. $B(\phi)$ is a coupling factor between dilaton field ϕ and complex scalar field Φ .

We concentrate our analysis on the probe limit, which corresponds to taking the limit as q approaches infinity. Under this particular condition, we can confidently assert that the gravity \mathcal{L}_g and matter sectors \mathcal{L}_m are effectively decoupled and described independently from one another. The equations of motion for the dilaton and the axions are obtained from \mathcal{L}_g as

$$\nabla^2\phi + 2\sqrt{3} \sinh\left(\frac{\phi}{\sqrt{3}}\right) = 0, \quad \nabla^2\psi_I = 0, \quad (2)$$

and the Einstein's equation becomes

$$R_{\mu\nu} - \frac{1}{2}g_{\mu\nu} \left[R - \frac{1}{2}(\partial\phi)^2 + 6 \cosh\left(\frac{\phi}{\sqrt{3}}\right) - \frac{1}{2} \sum_{I=1}^2 (\partial\psi_I)^2 \right] = \frac{1}{2}\partial_\mu\phi\partial_\nu\phi + \frac{1}{2} \sum_{I=1}^2 (\partial_\mu\psi_I\partial_\nu\psi_I). \quad (3)$$

Considering the metric ansatz

$$ds^2 = -f(r)dt^2 + \frac{dr^2}{f(r)} + h(r)(dx^2 + dy^2), \quad (4)$$

we obtain the following solution [43]

$$f(r) = r^2 \left(1 - \frac{P}{r}\right)^{1/2} \left(1 - \frac{k^2}{2r^2}\right), \quad h(r) = r^2 \left(1 - \frac{P}{r}\right)^{1/2}, \quad (5a)$$

$$\phi(r) = -\frac{\sqrt{3}}{2} \ln\left(1 - \frac{P}{r}\right), \quad \psi_I = (kx, ky), \quad (5b)$$

where P is an integration constant corresponding to the location of the curvature singularity at $r = P$ and it can be expressed in terms of temperature T and momentum dissipation strength k , see Eq. (6).¹ k is a positive constant of the linear axions, which can be understood as the strength of the momentum dissipation in the backreacted setup. Remark that k was introduced to break the translational symmetry. In this study, we naively expect that k still holds some aspects of the strength of the momentum dissipation, even in the probe limit. The geometry is a black hole spacetime with the horizon at $r = r_h = k/\sqrt{2}$. To avoid the naked singularity, the range of P is restricted by $-\infty < P < r_h$. In the probe limit, the gravity sector is decoupled from the Maxwell field. Therefore, this solution is a neutral black hole solution. Note that this solution was also studied in Refs. [48, 49], and Ref. [50] without the axions. This is also a special neutral case of the charged black hole studied in Refs. [43–46, 51]. (See also Appendix A). The authors of Ref. [46] studied the same model for general q beyond the probe limit. We call the above solution as ‘dilatonic black hole’. The Hawking temperature reads

$$T = \frac{r_h}{2\pi} \sqrt{1 - \frac{P}{r_h}}. \quad (6)$$

In order to obtain positive T , the range of P is restricted in $-\infty < P < r_h$.

On the other hand, the model also admits another neutral solution without the dilaton hair, which is given by [41]

$$f(r) = r^2 \left[1 - \frac{k^2}{2r^2} - \frac{r_h^3}{r^3} \left(1 - \frac{k^2}{2r_h^2} \right) \right], \quad h(r) = r^2, \quad \phi(r) = 0, \quad \psi_I = (kx, ky). \quad (7)$$

We call it as ‘bald black hole’ solution in this study. In this solution, k and r_h are independent parameters but the number of parameters does not change. Since the dilaton vanishes, the solution is same as the neutral solution in the linear axions model [41]. Now, the Hawking temperature is given by

$$T = \frac{1}{8\pi} \frac{6r_h^2 - k^2}{r_h}. \quad (8)$$

The range of k is restricted by $T > 0$ as $k < \sqrt{6}r_h$. This solution is thermodynamically favored in the range $T > \frac{k}{2\sqrt{2}\pi}$ [44, 48]. Therefore, we need to consider this solution as the background metric rather than the dilatonic black hole (5), at high temperatures where $T > k/(2\sqrt{2}\pi)$.

¹Note that the blackening factor is still different from $f(r) = r^2(1 - r_h^3/r^3)$ in the SAdS₄, even if one sets $P = 0$.

Under the probe limit, we can analyze the matter sector by considering the gravity, dilaton, and axions as non-dynamical background fields given by Eq. (5). For the matter sector, the equations of motion are obtained as

$$\nabla_\mu \left(e^{\frac{\phi}{\sqrt{3}}} F^{\mu\nu} \right) - iq\Phi^* (\partial^\nu - iqA^\nu) \Phi + iq\Phi (\partial^\nu + iqA^\nu) \Phi^* = 0, \quad (9)$$

$$D_\mu D^\mu \Phi - B(\phi)\Phi = 0. \quad (10)$$

We choose the mass term of Φ as

$$B(\phi) = M^2 \cosh(\tau\phi), \quad (11)$$

where M is a mass of the scalar field near $r = \infty$, and τ is a constant determining the coupling with the dilaton field. In this study, we fix $M^2 = -2$, which leads the dimension of the charged-scalar operator as $\Delta = 1$ or 2 . The authors of Ref. [46] indicate that the superconducting instability can be triggered easily at higher coupling τ . For more detail argument about $B(\phi)$, see Ref. [52]. Now, we consider the following ansatz:

$$\Phi = \Phi(r), \quad A = A_t(r) dt, \quad (12)$$

where $\Phi(r)$ can be considered as a real function. With the above ansatz, the equations of motion are written as

$$\Phi''(r) + \left(\frac{f'(r)}{f(r)} + \frac{h'(r)}{h(r)} \right) \Phi'(r) + \frac{1}{f(r)} \left(\frac{q^2 A_t(r)^2}{f(r)} - B(\phi) \right) \Phi(r) = 0, \quad (13)$$

$$A_t''(r) + \left(\frac{h'(r)}{h(r)} + \frac{\phi'(r)}{\sqrt{3}} \right) A_t'(r) - \frac{2e^{-\frac{\phi(r)}{\sqrt{3}}} q^2 \Phi(r)^2}{f(r)} A_t(r) = 0. \quad (14)$$

Near the boundary, these fields have the following asymptotic expansions

$$\Phi(r) = \frac{\Phi^{(1)}/\sqrt{2}}{r} + \frac{\Phi^{(2)}/\sqrt{2}}{r^2} + \dots, \quad (15)$$

$$A_t(r) = \mu - \frac{\rho}{r} + \dots. \quad (16)$$

For the vector field, μ and ρ are dual to the chemical potential and charge density of the boundary conformal field theory, respectively. For the scalar field, both the leading and the subleading terms can be normalizable in our case [53]. Similarly to Ref. [23], we refer the case when $\Phi^{(i)} = \langle O_i \rangle$ and $\Phi^{(j)} = 0$ as O_i theory, where $i = 1$ or 2 and $j \neq i$. The choice of the O_2 theory is called standard quantization, whereas the O_1 theory is realized by adding corresponding boundary action. $\langle O_i \rangle$ is considered as an operator with dimension i in the boundary theory.

For later convenience, we rewrite the coordinate by $z := r_h/r$. In this coordinate, the horizon is located at $z = 1$, and the boundary at $z = 0$. Under this transformation, Eqs. (13) and (14) become

$$\Phi''(z) + \left(\frac{2}{z} + \frac{f'(z)}{f(z)} + \frac{h'(z)}{h(z)} \right) \Phi'(z) + \frac{r_h^2}{z^4} \left(\frac{q^2 A_t(z)^2}{f(z)^2} - \frac{B(\phi(z))}{f(z)} \right) \Phi(z) = 0, \quad (17)$$

$$A_t''(z) - \frac{2e^{-\frac{\phi(z)}{\sqrt{3}}} q^2 r_h^2 \Phi(z)^2}{z^4 f(z)} A_t(z) = 0, \quad (18)$$

respectively. Note that the prime denotes the derivative with respect to z here.

3 Scaling relation between T_c and k

In this section, we investigate the phase boundaries by using both the numerical and analytic approximate methods. Using the approximate result, we find the linearly scaling relation between T_c and k as (32) for large k in the O_1 theory. We also present numerical results of the scalar condensation.

In the normal phase, i.e., $\Phi = 0$, Eq. (18) becomes

$$A_t''(z) = 0. \quad (19)$$

With the boundary condition (16) and $A_t(r_h) = 0$, the solution of this equation reads

$$A_t(z) = \mu(1 - z), \quad \mu = \frac{\rho}{r_h}, \quad (20)$$

where μ is an integration constant that can be read as the chemical potential in the boundary theory and ρ can be regarded as the charge density.

3.1 Phase boundaries

Below $T = T_c$, the normal phase solution will be unstable for the perturbation of the charged scalar. We investigate the phase boundaries by finding the onset of the scalar instability. In the z coordinate, the expansion of Φ is written as

$$\Phi(z) = \frac{\Phi^{(1)}}{\sqrt{2} r_h} z + \frac{\Phi^{(2)}}{\sqrt{2} r_h^2} z^2 + \dots \quad (21)$$

As we have mentioned, we have two choices of the normalizable modes. We consider the following ansatz of the perturbation for each theory. For the O_1 theory, we write $\Phi(z)$ as

$$\Phi(z) = \frac{\langle O_1 \rangle}{\sqrt{2} r_h} z F(z), \quad F(0) = 1, \quad F'(0) = 0. \quad (22)$$

For the O_2 theory, we write $\Phi(z)$ as

$$\Phi(z) = \frac{\langle O_2 \rangle}{\sqrt{2} r_h^2} z F(z), \quad F(0) = 0, \quad F'(0) = 1. \quad (23)$$

We also impose the regular condition for $F(z)$ at $z = 1$. The equation of motion (17) becomes

$$F''(z) + \left(\frac{4}{z} + \frac{f'(z)}{f(z)} + \frac{h'(z)}{h(z)} \right) F'(z) + \left(\frac{2}{z^2} + \frac{h'(z)}{zh(z)} + \frac{r_h^2 (q^2 A_t(z)^2 - B(\phi(z)) f(z))}{z^4 f(z)^2} + \frac{f'(z)}{zf(z)} \right) F(z) = 0. \quad (24)$$

This can be understood as the Sturm-Liouville (SL) problem. The equation in the SL form becomes

$$\frac{d}{dz} \{p(z)F'(z)\} + q(z)F(z) + \lambda r(z)F(z) = 0, \quad (25)$$

where

$$\begin{aligned} p(z) &= z^4 f(z) h(z), \\ q(z) &= z^3 f(z) h(z) \left(\frac{2}{z} + \frac{f'(z)}{f(z)} + \frac{h'(z)}{h(z)} \right) - r_h^2 B(\phi(z)) h(z), \\ r(z) &= \frac{(-1+z)^2 r_h^4 h(z)}{f(z)}, \quad \lambda = \frac{q^2 \mu^2}{r_h^2}. \end{aligned} \quad (26)$$

We can solve the above equation numerically. The minimum eigenvalue λ will correspond to the critical value of μ or T_c after rescaling parameters. Moreover, we can also study the approximation for the lowest eigenvalue, as follows. Supposing that Ψ_n is the eigenfunction for n -th eigenvalue $\lambda = \lambda_n$, we can formally write λ_n as

$$\begin{aligned}\lambda_n &= -\frac{\int_0^1 [\partial_z(p(z)\Psi_n'(z))\Psi_n(z) + q(z)\Psi_n(z)^2] dz}{\int_0^1 r(z)\Psi_n(z)^2 dz} \\ &= \frac{-p(z)\Psi_n(z)\Psi_n'(z)|_0^1 + \int_0^1 [p(z)\Psi_n'(z)^2 - q(z)\Psi_n(z)^2] dz}{\int_0^1 r(z)\Psi_n(z)^2 dz}.\end{aligned}\quad (27)$$

This is called Rayleigh Quotient. We leverage several properties of the Sturm-Liouville eigenvalue problem. One of them is the set of eigenfunctions is complete, i.e., $F(z) \sim \sum_{n=1}^{\infty} c_n \Psi_n(z)$. Thus, we can generalize this formula for a trial function $F(z)$ which is not a solution of the ordinary differential equation (25) but satisfies the boundary conditions. In this study, we consider trial functions with one parameter α denoted by F_α . In the SL problem, the smallest eigenvalue λ_1 always exists. Correspondingly, λ_α , associated with the trial function F_α , also has a minimum. We write

$$\hat{\lambda}_1 = \min_{\alpha} \frac{-p(z)F_\alpha(z)F_\alpha'(z)|_0^1 + \int_0^1 [p(z)F_\alpha'(z)^2 - q(z)F_\alpha(z)^2] dz}{\int_0^1 r(z)F_\alpha(z)^2 dz}.\quad (28)$$

This becomes an estimation for the actual smallest eigenvalue: $\hat{\lambda}_1 \approx \lambda_1$.

We have to note that the background spacetime also exhibits the phase transition between Eq. (5) and Eq. (7). Since we are working in the probe limit, this phase transition occurs at $T = k/(2\sqrt{2}\pi)$, regardless the charged-scalar instability. In the following, we first explore the charged-scalar instability in each background geometry. After that, we will show the correct phase boundaries as Fig. 3 by combining the results obtained in each geometry.

First, we consider the O_1 theory in each background geometry. We choose the following trial function with one parameter α in both background black-hole geometry:

$$F_\alpha(z) = 1 + \alpha z^2.\quad (29)$$

It satisfies the boundary conditions, $F(0) = 1$ and $F'(0) = 0$. We obtain the approximate formula for the minimal eigenvalue $\hat{\lambda}_1$. Figure 1 shows the phase boundaries in the $\frac{T_c}{q\mu} - \frac{k}{q\mu}$ plane obtained by the approximation, and also by the numerical way for comparison. Note that q can be scaled out in the probe limit analysis.² The approximation agrees with the numerical result well. Since the full expression of the approximation is too complicated, we do not exhibit it here. In the O_1 theory, the phase boundaries always lie in on $T > k/(2\sqrt{2}\pi)$ in each background geometry, as shown in Fig. 1. As a result, only the result in the bald black hole is relevant because the bald black hole is the ground state of the gravity sector when $T > k/(2\sqrt{2}\pi)$.

In the case of the bald black hole, the curve is parameterized by k/r_h in $0 < k/r_h < \sqrt{2}$. In $k/r_h \rightarrow \sqrt{2}$, the curve approaches to the dotted line denoting $T = k/(2\sqrt{2}\pi)$. In the case of the dilatonic black hole, the curves are parameterized by P/r_h in $-\infty < P/r_h < 0$, and small $|P|/r_h$ corresponds to large $\frac{k}{q\mu}$. Expanding the approximation for $\tau = 0$ in small $\epsilon \equiv -P/r_h$, we obtain

$$\lambda_{F_\alpha} = \frac{1}{4 \ln 2 - 2} \epsilon + \mathcal{O}(\epsilon^2).\quad (30)$$

²In the backreacted case, q can no longer be scaled out; different q explains different setups. Similar to the original model of the holographic superconductor, it is expected that the probe limit corresponds to $q \rightarrow \infty$ limit. See Appendix A.

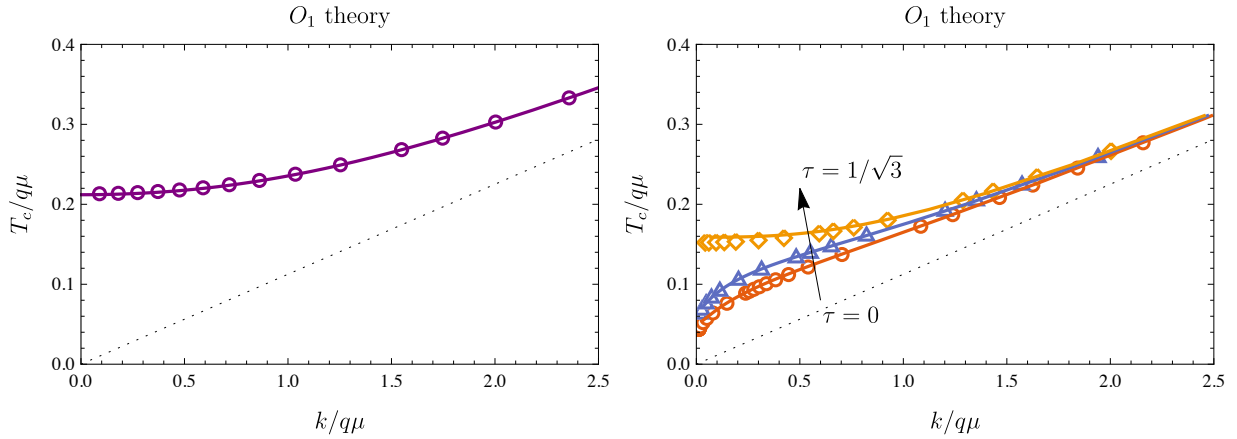


Figure 1: Superconducting phase boundaries in the $\frac{T_c}{q\mu} - \frac{k}{q\mu}$ plane for the O_1 theory in the two different black hole solutions. The black dotted lines show $T = k/(2\sqrt{2}\pi)$ where the phase transition of the background spacetime occurs. (left) The result in the bald black hole (7). (right) the result in the dilatonic black hole (5). The curves show the SL approximations while the points show the direct numerical results. In the right panel, the results depend on τ . The curves and data correspond to $\tau = 0, \frac{5}{4}, \frac{1}{\sqrt{3}}$ from bottom to top.

Using this leading expansion, $\frac{T_c}{q\mu}$ and $\frac{k}{q\mu}$ can be written as

$$\frac{T_c}{q\mu} = \frac{\sqrt{\ln 2 - 1/2}}{\pi} \epsilon^{-1/2} + \mathcal{O}(\epsilon^{1/2}), \quad \frac{k}{q\mu} = 2\sqrt{2\ln 2 - 1} \epsilon^{-1/2} + \mathcal{O}(\epsilon^{1/2}). \quad (31)$$

We obtain the scaling relation for large k as

$$T_c \approx \frac{k}{2\sqrt{2}\pi}. \quad (32)$$

T_c approaches to the critical value of the phase transition of the background spacetime. In the case of the bald black hole, T_c approaches to this value for large k , too. It can be also confirmed from the numerical results for $\frac{T_c}{q\mu}$ at large $\frac{k}{q\mu}$ (, see Fig. 1). This result illustrates the critical temperature is directly proportional to the momentum dissipation strength in the O_1 theory. Comparable outcomes were indeed numerically established in the studies of [54] and [46], yet these works did not explicitly elucidate or demonstrate such findings within the regime transcending the probe limit (refer to Figure 1 presented in both [54] and [46] for a clearer understanding).

Next, we consider the O_2 theory in each background geometry. In the bald black hole, we employ a simple trial function with one parameter,

$$F_\alpha = z(1 + \alpha z). \quad (33)$$

In this case, the curve is parameterized by k/r_h in $0 < k/r_h < \sqrt{6}$. In the dilatonic black hole, however, this simple trial function does not work well. We find that the following trial function with one parameter α , gives rational results for the wider range of k/μ in this case. It is given by

$$F_\alpha(z) = z(1 + \alpha z) \left(1 - \frac{Pz}{r_h}\right)^{-\frac{\sqrt{3}}{2}\tau}. \quad (34)$$

This trial function satisfies $F(0) = 0$ and $F'(0) = 1$ so it is suitable for studying the O_2 theory.³ The exponential factor $-\frac{\sqrt{3}}{2}\tau$ is just same as those involved in the coupling term $B(\phi)$, see Eq. (11).

³One can also consider $F_\alpha = \frac{z(1+\alpha z)}{1+z} \left(1 - \frac{Pz}{r_h}\right)^{-\frac{\sqrt{3}}{2}\tau}$, which gives good agreement too.

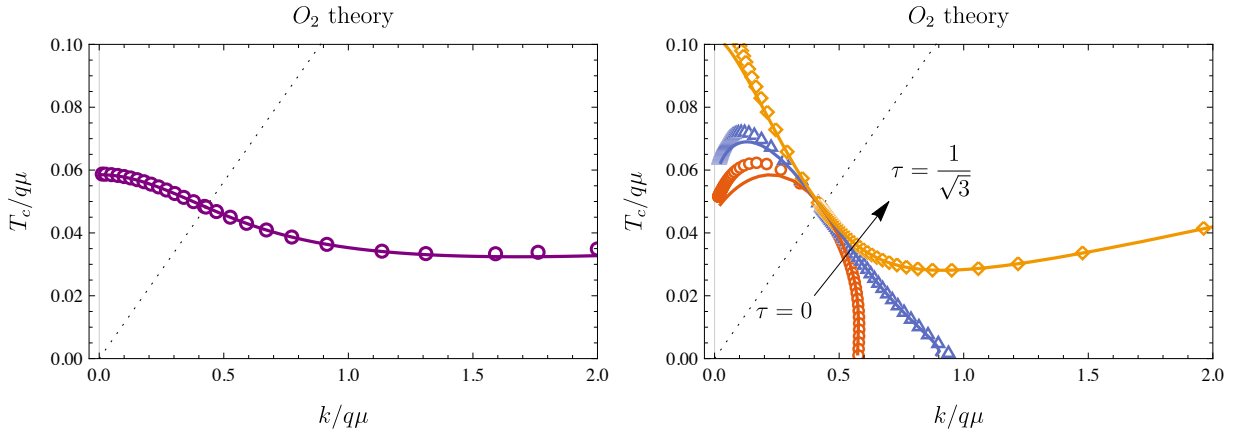


Figure 2: Superconducting phase boundaries in the $\frac{T_c}{q\mu} - \frac{k}{q\mu}$ plane for O_2 -theory in the two different black hole solutions. The black dotted lines show $T = k/(2\sqrt{2}\pi)$ where the phase transition of the background spacetime occurs. (left) The result in the bald black hole (7). (right) The result in the dilatonic black hole (5). The curves show the SL approximations, while the points show numerical results obtained directly. In the right panel, the results depend on τ . The curves and data correspond to $\tau = 0$, $\frac{3}{4\sqrt{3}}$ and $\frac{1}{\sqrt{3}}$ from bottom to top.

Figure 2 shows the results of the phase boundaries in the $\frac{T_c}{q\mu} - \frac{k}{q\mu}$ plane obtained by the approximation and the numerical method, for a comparison. The approximation almost agrees with the numerical result. Unlike the O_1 theory, the curves cross the line of $T = k/(2\sqrt{2}\pi)$, and T_c reaches zero if τ is small. In the case of the dilatonic black hole, the curves are parameterized by P/r_h , but it can take a value in $0 < P/r_h < 1$ in the O_2 theory. At $P/r_h = 0$, the result does not depend on τ which is located at $(\frac{k}{q\mu}, \frac{T_c}{q\mu}) \approx (0.41, 0.049)$ on the dotted line. For large enough τ , T_c linearly depends on k but the coefficient is different from Eq. (32). For $\tau = 1/\sqrt{3}$, we numerically obtain $T_c \approx 0.0193k$ for large k . Such behavior in $T < k/(2\sqrt{2}\pi)$ is qualitatively same as those studied in Ref. [46].

Finally, we show the correct phase boundaries for each theory. Combining the results in Fig. 1 for the O_1 theory, and Fig. 2 for the O_2 theory, we obtain the phase boundaries as Fig. 3. According to the critical value of $T = k/(2\sqrt{2}\pi)$, which is shown as the dotted line, we have switched the using background geometry and the corresponding results. Note that the purple curves in $T > k/(2\sqrt{2}\pi)$ are independent of the choice of τ because τ represents a coupling with the dilaton. For the O_1 theory, we employed only the purple curve corresponding to the bald black hole because all curves are located in $T > k/(2\sqrt{2}\pi)$. The result for the O_2 theory corresponds to the fully backreacted result in Ref. [46]. We also provide further comparisons with the full analysis in Appendix A. The calculation of the critical temperature T_c in this study demonstrates that employing the probe limit yields coherent and meaningful results by duly considering the phase transition dynamics within the background gravity sector.

For both the O_1 theory and the O_2 theory with substantial τ values, it is revealed that T_c increases as the parameter k grows at high k regimes. Specifically, for the O_1 theory, the large- k behavior can be effectively approximated using Eq. (32). Although initially, this positive correlation between T_c and k , which signifies the strength of momentum dissipation, may seem counter-intuitive, such a trend has been consistently observed across various holographic models incorporating k [46, 54], as previously discussed. In light of these findings, a future discourse on the validity and implications of this scaling relationship between T_c and k from the perspective of condensed matter physics would indeed be valuable and insightful. It remains to be explored whether this phenomenon aligns with physical expectations or presents novel challenges to our current understanding.

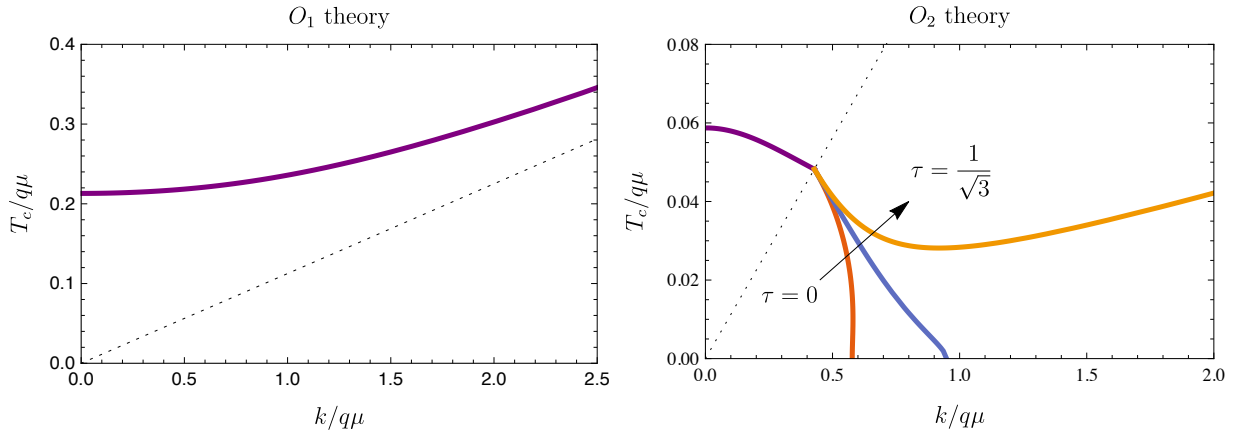


Figure 3: Correct superconducting phase boundaries for each theory. The black dotted lines show $T = k/(2\sqrt{2}\pi)$. The purple curves in $T > k/(2\sqrt{2}\pi)$ show the numerical results in the bald black hole. The other curves in $T < k/(2\sqrt{2}\pi)$ show the numerical results in the dilatonic black hole for various τ . We have showed only the relevant results by taking the phase transition of the background geometry into account. In the right panel, the curves in $T < k/(2\sqrt{2}\pi)$ correspond to $\tau = 0, \frac{3}{4}, \frac{1}{\sqrt{3}}$ from bottom to top, respectively.

3.2 Condensation

In the superconducting phase, the charged scalar has nontrivial profiles below $T = T_c$. The scalar profile is obtained by solving the nonlinear ODEs for Φ and A_t . We conclude this section by showing the numerical results of the condensations for O_1 and the O_2 theory. Here, we set $q = 1$ but the choice of q does not affect the results in the probe limit since it can be scaled out.

Figure 4 shows the condensates $\langle O_i \rangle$ as functions of T for O_i theories. We set $\tau = 0$ for simplicity. To obtain this figure, we have changed the using background geometry at the phase transition point $T = k/(2\sqrt{2}\pi)$. We show this point as a small circle on the curve, if it exists below the superconducting phase transition point. The condensate $\langle O_1 \rangle$ grows as temperature decreases, whereas $\langle O_2 \rangle$ remains finite at $T \rightarrow 0$. In particular, there is a lower bound for the possible T in the O_1 theory. This behavior is same as those studied in [23], and is a limitation in the probe limit analysis.⁴ Since the lowest temperature is always larger than $T = k/(2\sqrt{2}\pi)$ for the O_1 theory, the results in the bald black hole, denoted as solid curves, are favored. We expect that the low-temperature divergence of $\langle O_1 \rangle$ will be cured by considering beyond the probe limit, similarly to Ref. [24]. One can see that $\langle O_1 \rangle$ is enhanced by increasing k for fixed μ . On the other hand, $\langle O_2 \rangle$ is suppressed as k increases. These behaviors of the condensates are consistent with the relation between T_c and k for each theory, shown as Fig. 3.

4 Linear dependence of T_c on the superfluid density

In Ref. [15], the authors reveal the dependence of critical temperature (T_c) in overdoped copper oxide superconductors, specifically $\text{La}_{2-x}\text{Sr}_x\text{CuO}_4$, on their superfluid density. Using atomic layer molecular beam epitaxy, homogeneous single-crystal films with varying doping levels were synthesized to thoroughly investigate the entire overdoped region. The team measured magnetic penetration depth and zero temperature phase stiffness with high precision across thousands of samples. Results showed a consistent linear decrease of phase stiffness with temperature at all doping levels. In this section, we compute the AC conductivity in our model to investigate the relation between T_c

⁴In the O_2 theory with $\tau = 0$, $T \rightarrow 0$ limit is possible.

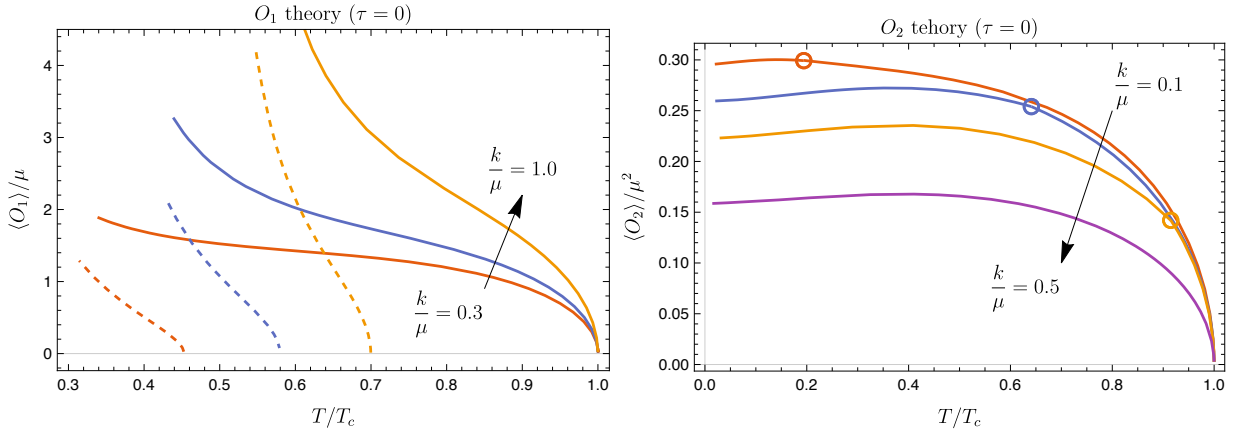


Figure 4: Condensation as functions of T for various k/μ . We set $\tau = 0$. (left) For the O_1 theory. The solid and dashed curves show the results in the bald and the dilatonic black hole, respectively. $\langle O_1 \rangle / \mu$ grows as the temperature decreases. We obtain the data for $T > k/(2\sqrt{2}\pi)$, i.e., the solid curves are favored. The solid (dashed) curves correspond to $k/\mu = 0.3, 0.6$ and 1.0 from bottom to top. (right) For the O_2 theory. The curves correspond to $k/\mu = 0.1, 0.3, 0.4$ and 0.5 , from top to bottom. The small circles on the curves indicates the critical point at $T = k/(2\sqrt{2}\pi)$. Below/above the temperature of this point, the data is obtained with the dilatonic/bald black hole, respectively. For $k/\mu = 0.5$, all data are obtained in the dilatonic black hole because $T_c < k/(2\sqrt{2}\pi)$ in this case. Unlike the O_1 theory, $\langle O_2 \rangle / \mu^2$ remains finite at $T \rightarrow 0$.

and the zero-temperature superfluid density $n_s(0)$. The exact AC conductivity in the dilatonic black hole, in which corresponds to the normal phase, was studied in Ref. [49]. The superfluid density n_s can be read from the AC conductivity in the superconducting phase. We numerically compute the AC conductivity in the superconducting phase. As a result, we find the linear relation between T_c and $n_s(0)$ in the O_2 theory. We also provide the approximate formula for the AC conductivity in the superconducting phase in our model.

In order to compute the AC conductivity, we need to solve Eq. (9) for the following perturbation ansatz

$$A = A_t(r)dt + e^{-i\omega t} A_x(r)dx, \quad (35)$$

where $A_x(r)$ is a small perturbation field. Linearizing Eq. (9) about $A_x(r)$, we obtain

$$A_x''(r) + \left(\frac{f'(r)}{f(r)} + \frac{\phi'(r)}{\sqrt{3}} \right) A_x'(r) + \left(\frac{\omega^2}{f(r)^2} - \frac{2q^2 e^{-\frac{\phi(r)}{\sqrt{3}}}}{f(r)} \Phi(r)^2 \right) A_x(r) = 0. \quad (36)$$

In the z -coordinate, it becomes

$$A_x''(z) + \left(\frac{2}{z} + \frac{f'(z)}{f(z)} + \frac{\phi'(z)}{\sqrt{3}} \right) A_x'(z) + \frac{r_h^2 \left(\omega^2 - 2e^{-\frac{\phi(z)}{\sqrt{3}}} q^2 f(z) \Phi(z)^2 \right)}{z^4 f(z)^2} A_x(z) = 0. \quad (37)$$

To obtain the physical result of the AC conductivity, we impose the infalling-wave boundary condition at the black hole horizon. From the equation of motion, the infalling-wave solution must have the near horizon behavior written as

$$A_x(z) = (1-z)^{\frac{-i\omega}{4\pi T}} G(z), \quad (38)$$

where $G(z)$ is a regular function at the horizon $z = 1$. According to the prescription of the AdS/CFT correspondence with finite temperatures [55], we can compute the AC conductivity by

$$\sigma(\omega) = -\frac{1}{i\omega} \lim_{r \rightarrow \infty} \frac{r^2 \partial_r A_x(r)}{A_x(r)} = \frac{r_h}{i\omega} \lim_{z \rightarrow 0} \frac{\partial_z A_x(z)}{A_x(z)}. \quad (39)$$

In the following, we study the AC conductivity in our model by using both the numerical and the analytical approximate methods in each phase.

4.1 AC conductivity in the normal phase

We now offer a concise analysis by deriving the exact mathematical formulas for AC conductivity within the normal phase. The normal phase is described by $\Phi(r) = 0$, then Eq. (36) becomes

$$A_x''(r) + \left(\frac{f'(r)}{f(r)} + \frac{\phi'(r)}{\sqrt{3}} \right) A_x'(r) + \frac{\omega^2}{f(r)^2} A_x(r) = 0. \quad (40)$$

Using the dilatonic black hole geometry (5), the equation has regular singular points at $r = \pm r_h$ and P . The solution is given by

$$A_x(r) = C_0 \left(\frac{r - r_h}{r + r_h} \right)^{-i\omega/4\pi T} {}_2F_1 \left(\tilde{a}, \tilde{b}; \tilde{c}; \tilde{x} \frac{r - r_h}{r + r_h} \right), \quad (41)$$

where C_0 is a normalization constant, and

$$\begin{aligned} \tilde{a} &= -\frac{i\omega}{2r_h} \left(\frac{1}{\sqrt{1 - P/r_h}} - \frac{1}{\sqrt{1 + P/r_h}} \right), & \tilde{b} &= -\frac{i\omega}{2r_h} \left(\frac{1}{\sqrt{1 - P/r_h}} + \frac{1}{\sqrt{1 + P/r_h}} \right), \\ \tilde{c} &= 1 - \frac{i\omega/r_h}{\sqrt{1 - P/r_h}}, & \tilde{x} &= \frac{P + r_h}{P - r_h}. \end{aligned} \quad (42)$$

Note that this solution is exactly same as those obtained in Ref. [49] for the 3-charge black hole. The form of the expression can be exchanged by using the property of the hypergeometric function. Using Eq. (39), the AC conductivity is obtained as

$$\sigma(\omega) = \frac{1}{\sqrt{1 - P/r_h}} - \frac{r_h}{i\omega} \frac{2\tilde{a}\tilde{b}\tilde{x}}{\tilde{c}} \times \frac{{}_2F_1(1 + \tilde{a}, 1 + \tilde{b}; 1 + \tilde{c}; \tilde{x})}{{}_2F_1(\tilde{a}, \tilde{b}; \tilde{c}; \tilde{x})}. \quad (43)$$

We show the results of Eq. (43) in some cases in Fig. 5. From this expression, we can read off the DC conductivity as

$$\sigma_{\text{DC}} = \lim_{\omega \rightarrow 0} \sigma(\omega) = \frac{1}{\sqrt{1 - P/r_h}} = \frac{1}{2\sqrt{2\pi}} \frac{k}{T}. \quad (44)$$

The result agrees with the DC conductivity obtained in Refs. [45, 46] with vanishing chemical potential, i.e., in the neutral limit. To obtain the ω -dependent AC conductivity and the T -dependent DC conductivity, the nonzero dilaton and the coupling between the dilaton and the Maxwell field are important [49]. If the theory has the S-duality, the conductivity becomes constant as those in the bald black hole that we will show next. For more details about this point, see Ref. [56] and section 3.4.6 of Ref. [57]. We can say that the presence of the non-zero dilaton plays a significant role for the emergence of the linear- T resistivity here.

The above result is valid only during the dilatonic black hole (5) is the true ground state at low temperature. If the bald black hole (7) becomes the ground state, the infalling-wave solution for A_x in this geometry is obtained as

$$\begin{aligned} A_x(z) &= C_0 (1 - z)^{-\frac{i\omega}{4\pi T}} \left(2 + 2z + (2 - \tilde{k}^2)z^2 \right)^{\frac{i\omega}{8\pi T}} \left(\frac{i\sqrt{3 - 2\tilde{k}^2} - 1 - (2 - \tilde{k}^2)z}{i\sqrt{3 - 2\tilde{k}^2} + 1 + (2 - \tilde{k}^2)z} \right)^{\lambda'}, \\ \lambda' &= \frac{3 - \tilde{k}^2}{\sqrt{3 - 2\tilde{k}^2}} \frac{\omega}{8\pi T}, \end{aligned} \quad (45)$$

where $\tilde{k} = k/r_h$. Note that T is given by Eq. (8) in the bald black hole. In this case, however, one obtains the conductivity as $\sigma(\omega) = 1$ for any ω . Thus, the DC conductivity is also given by $\sigma_{\text{DC}} = 1$. As a result, the (DC) resistivity behaves

$$\rho_{\text{DC}} = \frac{1}{\sigma_{\text{DC}}} = \begin{cases} 0 & T \leq T_c \\ 2\sqrt{2}\pi T/k & T_c < T \leq k/(2\sqrt{2}\pi) \\ 1 & k/(2\sqrt{2}\pi) < T \end{cases} \quad (46)$$

If T_c is larger than $k/(2\sqrt{2}\pi)$, the middle regime disappears. ρ_{DC} does not jump at $T = k/(2\sqrt{2}\pi)$ because Eq. (44) becomes 1 there. The behavior of Eq. (46) actually corresponds to the result in the full analysis with backreactions [45].

4.2 Numerical results for the AC conductivity in the SC phase

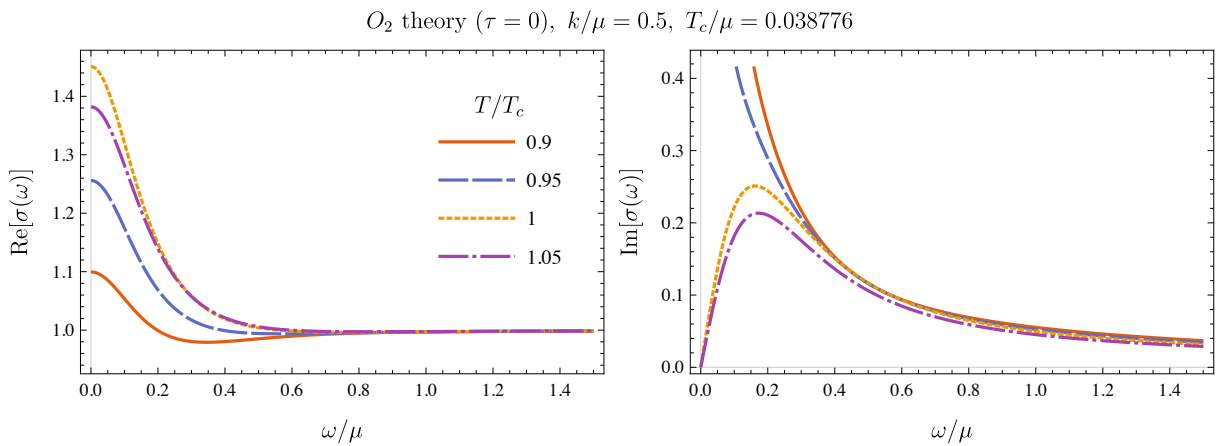


Figure 5: AC conductivity for $k/\mu = 0.5$ around the critical temperature in the O_2 theory. Above T_c , the result is given by Eq. (43). Below T_c , the result is obtained numerically. One can see the $1/\omega$ dependence implying the superconductivity in the imaginary part of the conductivity for $T < T_c$.

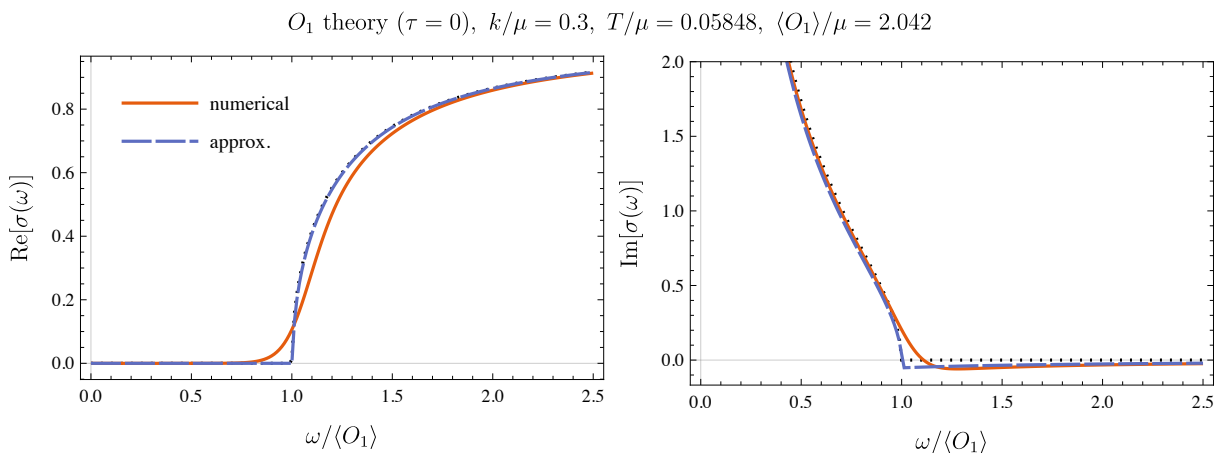


Figure 6: AC conductivity for $k/\mu = 0.3$ of the O_1 theory in the dilatonic black hole. The red curve shows the numerical result, and the blue dashed curve shows the approximation given by Eq. (59). The black dotted curve, which is almost overlapped by the blue dashed curve, shows Eq. (60).

In the superconducting phase, we need the numerical analysis to study the AC conductivity basically. With the benefit of the simplification in the probe limit, we can easily compute it by using the standard procedure in the holography. Figure 5 shows the AC conductivity in the O_2 theory with $\tau = 0$ for $k/\mu = 0.5$ and various T near T_c . Note that $T_c < k/(2\sqrt{2}\pi)$ in this case. We can use the dilatonic black hole as the background geometry. In the superconducting phase, below T_c , we can observe $1/\omega$ dependence in the imaginary part of the AC conductivity, which implies the delta peak in the real part.

Figure 6 shows the AC conductivity in the O_1 theory in the dilatonic black hole. Note that the true ground state is the bald black hole since $T > k/(2\sqrt{2}\pi)$. We show this plot for the purpose of showing how the AC conductivity behaves if the dilatonic black hole is favored. For the purpose of comparing with the approximation we will explore later, we have scaled ω by $\langle O_1 \rangle$ here. At the low temperature, the real part of the conductivity exhibits the gap-like structure. This behavior is similar to those in the original model of the holographic superconductor.

Another interesting observable in the superconducting phase is the superfluid density n_s , which is also called phase stiffness. This quantity can also be understood as the order parameter of the superconducting phase. It can be read from the low-frequency expansion of the AC conductivity as⁵

$$\sigma(\omega) = \pi n_s \delta(\omega) + \frac{in_s}{\omega} + \mathcal{O}(\omega). \quad (47)$$

Remark that the real and the imaginary parts of the conductivity are related with each other by the demand of the causality.⁶ Figure 7 shows the numerical results of n_s as functions of T for various k . The behavior of n_s is similar to $\langle O_i \rangle$ at low temperatures, see Fig. 4. Unlike Fig. 4, we can see from the numerical results that $n_s(T)$ has linear behavior near $T = T_c$.

In the O_2 theory with $\tau = 0$, n_s remains finite in the vicinity of $T = 0$ even in the probe limit analysis. Figure 8 shows the relation between n_s at $T = 0$ and T_c in the O_2 theory with $\tau = 0$. We find $n_s(0)$ and T_c have weakly linear relation as shown in this figure. The relation can be fitted by

$$n_s(0) \sim 0.159T_c + 0.00778\mu, \quad (48)$$

which is shown as the dashed line in Fig. 8. The similar scaling relation is known as the Uemura relation for underdoped materials [58, 59]. It was also observed in the overdoped side of copper oxides [15]. On the other hand, there is a universal scaling law between $n_s(0)$ and T_c known as Homes' law given by $n_s(0) \propto \sigma_{\text{DC}}(T_c) \times T_c$ in unconventional superconductors [60, 61]. Our result shows the linear relation between $n_s(0)$ and T_c but σ_{DC} given by Eq. (44) must enter here. Hence, the Homes' law is not held. We should note we are studying the probe limit. The test of the Homes' law in the fully backreacted setup in the Gubser-Rocha model was studied in [46].

Regarding Fig. 8, several significant points merit attention. First, it is crucial to note that the precise zero-temperature limit in our geometry presents a subtle issue because the horizon and singularity converge at a single point. To estimate $n_s(0)$, we rely on numerical AC conductivity data for a near-zero temperature scenario with $P/r_h = 0.99999$ because $P/r_h = 1$ corresponds to

⁵ n_s defined in (47) may be called as the phase stiffness rather than the superfluid density in some studies. In fact, the dimension of n_s is 1, which is different from the dimension of the number density. The number density of the super-fluid components, ρ_s , might be given by $n_s = \rho_s/m^*$, where m^* denotes the effective mass of the charged carrier. In the holographic superconductor models, one may take $m^* = \mu$. See, e.g., section 6.4.1 of Ref. [57] for more details.

⁶It is known as the Kramers-Kronig relation

$$\text{Im}[\sigma(\omega)] = -\frac{1}{\pi} \mathcal{P} \int_{-\infty}^{\infty} d\omega' \frac{\text{Re}[\sigma(\omega')]}{\omega' - \omega}, \quad \text{Re}[\sigma(\omega)] = \frac{1}{\pi} \mathcal{P} \int_{-\infty}^{\infty} d\omega' \frac{\text{Im}[\sigma(\omega')]}{\omega' - \omega},$$

where \mathcal{P} denotes taking the Cauchy's principal value of the integral.

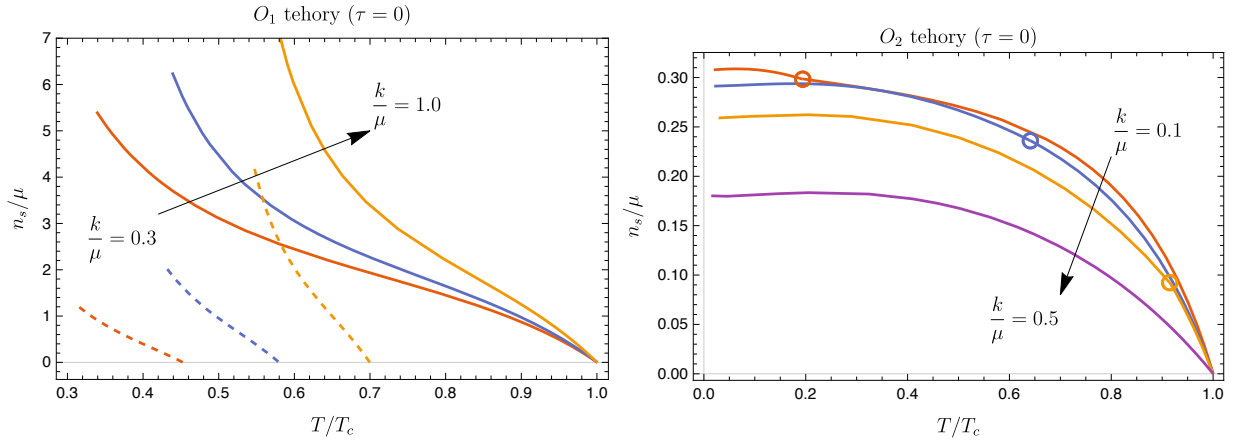


Figure 7: Superfluid density as functions of T for various k/μ . We set $\tau = 0$. (left) For the O_1 theory. (right) For the O_2 theory. The curves corresponds to those shown in Fig. 4. The behavior of n_s is very similar to the behavior of $\langle O_i \rangle$. A different point is that $n_s(T)$ goes zero linearly near $T = T_c$.

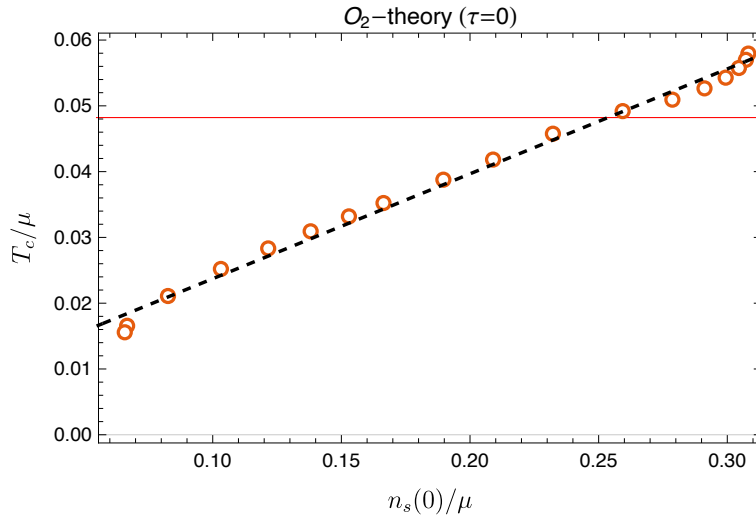


Figure 8: Relation between T_c and $n_s(0)$ in the O_2 theory with $\tau = 0$. $n_s(0)$ is defined by $n_s(0) = \lim_{T \rightarrow 0} n_s(T)$. We find $n_s(0)$ and T_c exhibit the linear relation roughly. The black dashed line shows the fit (48). The horizontal red line shows the critical point $T_c/\mu = 0.048218$ where $2\pi T_c = k/\sqrt{2}$ is satisfied. Above this line, we use T_c obtained by using the bald black hole, which is thermodynamically favored.

$T = 0$ from Eq. (6). The empirical values are obtained from solutions where the temperature is approximately an order of $T/T_c \sim 10^{-3}$.

Secondly, for very small critical temperatures T_c , the relationship between $T_c(k)$ and k becomes multivalued within a narrow range of k . Consequently, there is ambiguity about which value of $n_s(0)|_k$ corresponds to which specific $T_c(k)$. Due to this complexity, we have omitted the small T_c data from Fig. 8.

Lastly, the background spacetime undergoes a phase transition. In Fig. 8, the red horizontal line denotes the critical threshold corresponding to $T = k/(2\sqrt{2}\pi)$. Above this line, the bald black hole described by Eq. (7) represents the stable ground state. The data points presented in Fig. 8 inherently account for this phase transition.

4.3 Approximation for the AC conductivity in the SC phase

In this section, we delve into the derivation of an approximate expression for the AC conductivity within the superconducting phase that utilizes the dilatonic black hole geometry as given by Eq.(5). For this purpose, we employ the method developed in Ref. [25].⁷

We focus on the O_1 -theory. In this case, Φ is written as

$$\Phi(z) = \frac{\langle O_1 \rangle}{\sqrt{2}} \frac{z}{r_h} F(z), \quad (49)$$

satisfying $F(0) = 1$ and $F'(0) = 0$. In the superconducting phase, the vector perturbation equation is given by Eq. (36). Rewriting $A_x(r) = e^{-\frac{\phi(r)}{2\sqrt{3}}} B_x(r)$, we obtain

$$B_x''(r) + \frac{f'(r)}{f(r)} B_x'(r) + \frac{\omega^2}{f(r)^2} B_x(r) = \left[\frac{2q^2 e^{-\frac{\phi(r)}{\sqrt{3}}}}{f(r)} \Phi(r)^2 + \frac{1}{2\sqrt{3}} \left(\frac{f'(r)}{f(r)} \phi'(r) + \frac{\phi'(r)^2}{2\sqrt{3}} + \phi''(r) \right) \right] B_x(r). \quad (50)$$

Now, we consider the tortoise coordinate

$$r_* = \int_{r_h}^r \frac{dr}{f(r)} = \frac{1}{2r_h \sqrt{1 - P/r_h}} \ln |r - r_h| - \frac{\sqrt{1 - P/r_h}}{4(P - r_h)^2} (r - r_h) + \dots \quad (51)$$

In this coordinate, the horizon is located at $r_* = -\infty$, and the boundary is located at $r_* = 0$. Note that r_* can be written as $r_* \approx -z/r_h$ near the boundary. By using this coordinate, Eq. (50) can be written as

$$\ddot{B}_x(r_*) + \omega^2 B_x(r_*) = V(r) B_x(r_*), \quad (52)$$

where the dot denotes ∂_{r_*} , and V is given by

$$V(r) = 2q^2 e^{-\phi/\sqrt{3}} f \Phi^2 + \frac{f^2}{2\sqrt{3}} \left(\frac{f'}{f} \phi' + \frac{\phi'^2}{2\sqrt{3}} + \phi'' \right). \quad (53)$$

The values of the potential at the horizon and boundary are

$$V(r_h) = 0, \quad V(\infty) \equiv V_\infty = q \langle O_1 \rangle^2 + \frac{3}{16} P^2, \quad (54)$$

respectively. Figure 9 shows the shapes of the potential for various $T/\langle O_1 \rangle$ in the O_1 theory.

⁷We also present another approximate formula in Appendix B.

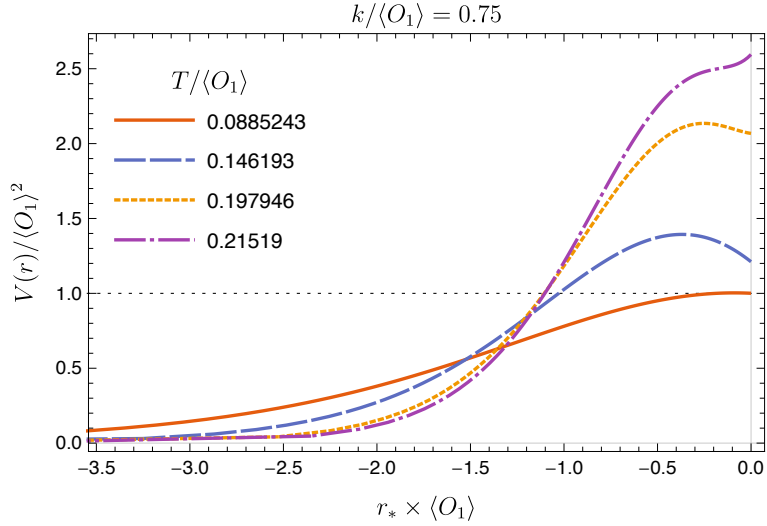


Figure 9: Potential (53) for various $T/\langle O_2 \rangle$ in the O_1 theory. We set $q = 1$ and $k/\langle O_1 \rangle = 0.75$. The dotted horizontal line shows $V(r)/\langle O_1 \rangle^2 = 1$.

To solve (52), we utilize the approximate method developed in [25]. Now, we consider replacing $V(r)$ in Eq. (52) with a ‘mean value’ denoted by \bar{V} which is a r -constant. Assuming $\omega^2 > \bar{V}$, we obtain the infalling wave solution as

$$B_x(r_*) = C \exp\left(i\sqrt{\omega^2 - \bar{V}}r_*\right), \quad (55)$$

where C is a normalization constant. The ‘mean value’ is defined by

$$\bar{V} = \frac{\int_{-\infty}^0 dr_* V(r) |B_x(r_*)|^2}{\int_{-\infty}^0 dr_* |B_x(r_*)|^2}. \quad (56)$$

The integrals diverge due to the infinite volume of the integral region. It will be regularized by introducing a large cutoff.⁸ In this study, however, we just consider only the leading contribution at $r = \infty$:

$$\bar{V} = V_\infty = q\langle O_1 \rangle^2 + \frac{3}{16}P^2. \quad (57)$$

This choice will be valid in a case where $r_h \ll \langle O_1 \rangle$. Using this result, A_x is approximated as

$$A_x(r_*) \approx C \exp\left(i\sqrt{\omega^2 - q\langle O_1 \rangle^2 - \frac{3}{16}P^2}r_* - \frac{\phi(r)}{2\sqrt{3}}\right). \quad (58)$$

According to the standard prescription of the AdS/CFT correspondence [55], and the Kubo formula, the conductivity is obtained as

$$\sigma(\omega) \approx i\frac{P}{4\omega} + \sqrt{1 - \frac{\frac{3}{16}P^2 + q^2\langle O_1 \rangle^2}{\omega^2}}. \quad (59)$$

If $P = 0$, the above result reduces to the approximate formula in the original model of the holographic superconductor, which is given by [25, 26]

$$\sigma(\omega) \approx \sqrt{1 - \frac{q^2\langle O_1 \rangle^2}{\omega^2}}. \quad (60)$$

⁸In [25], they considered it can be regularized by inserting a small imaginary part of ω .

Although the infalling boundary condition is only valid for $|\omega| > \sqrt{V}$, the approximate formula can fit even in a small ω region. Expanding Eq. (59) in small ω , we obtain the superfluid density as

$$n_s \approx \frac{P}{4} + \sqrt{\frac{3}{16}P^2 + q^2\langle O_1 \rangle^2}, \quad T \ll \langle O_1 \rangle. \quad (61)$$

Note that P is written in terms of k and T as $P = k/\sqrt{2} - 4\sqrt{2}\pi^2 T^2/k$. Thus, this is a function of T, k and $\langle O_1 \rangle$.

For a comparison, we show Eqs. (59) and (60) with the numerical result, for a specific background solution, in Fig. 6. The background solution is parameterized by $P/r_h = -2$, and its temperature is almost $T/T_c = 0.60$. While the temperature is not sufficiently low, the AC conductivity roughly exhibits the gap. In this case, the gap of the value is almost given by $\omega \approx \langle O_1 \rangle$, and the curves for Eq. (59) and Eq. (60) are almost overlapping. Eq. (61) also gives $n_s/\langle O_1 \rangle \approx 0.9521$, while the numerical result gives $n_s/\langle O_1 \rangle \approx 0.9710$. From Eq. (60), the the superfluid density can be read as $n_s/\langle O_1 \rangle = 1$. Indeed, Eq. (59) can be said as a better approximation than Eq. (60) but the correction is very small and difficult to see in Fig. 6. Note that Fig. 6 corresponds to the solution above $T = k/(2\sqrt{2}\pi)$ so the solution with the dilatonic black hole is not favored actually. We could not obtain the superconducting solution in $T < k/(2\sqrt{2}\pi)$, where the dilatonic black hole is the ground state, for the O_1 theory.

5 Discussion and Conclusion

To unravel the intricate scaling relations in holographic superconductors, this study has delved into an investigation of the Gubser-Rocha model within the probe limit framework. This approach has enabled us to examine various fundamental aspects of the holographic superconductor model. We have shown the several properties of the holographic superconductor model, e.g., the critical temperature T_c , the condensations $\langle O_i \rangle$, and also the AC conductivity $\sigma(\omega)$ in both phases. In the analysis of the critical temperature, we have found the scaling relation (32) between T_c and k for the O_1 theory. We have also studied the relation between T_c and the superfluid density n_s at zero temperature in the O_2 theory. They exhibit the linear relation similar to the recent experiment of the high T_c superconductors [15]. We have also studied the approximate formula for the AC conductivity in the O_1 theory.

The linear relation between T_c and the zero-temperature superfluid density $n_s(0)$ is known as the Uemura relation [58, 59]. The Uemura relation works reasonably for underdoped materials. The recent experiment also showed the similar relation in the overdoped materials [15]. Our result may imply that the O_2 theory with $\tau = 0$ of our model can describe such cuprates. On the other hand, the Homes' law [60, 61] is known as the universal scaling relation, which works regardless of whether overdoped or underdoped materials. This relation is expressed as $n_s(0) \propto \sigma_{\text{DC}}(T_c)T_c$. The Homes' law involves the normal phase DC conductivity at $T = T_c$ which will be inaccurate in the probe limit. Thus, this universal relation is not suitable for checking the model within the probe limit analysis. The Homes' law in the holographic superconductor model was tested in Ref. [46] in the analysis with backreactions. They concluded that the Homes' law holds in the O_2 theory with sufficiently large τ in this model. We have to note that the material in Ref. [15] violates the Homes' law. It was discussed in Ref. [62].

Our primary emphasis lies on the superfluid density; however, the behavior of the normal fluid density plays a vital role in high-temperature superconductors. Recent studies [63, 64] have uncovered that in certain classes of holographic superconductors, the normal fluid density persists even down to absolute zero temperature—a phenomenon starkly contrasting the predictions of BCS theory, wherein the normal fluid density vanishes at zero temperature. According to [64], this unconventional persistence occurs when the dynamical exponent z exceeds the sum of $d + 2$, where

$d + 1$ represents the spacetime dimension of the boundary theory. Given that the Gubser-Rocha black hole corresponds to $z \rightarrow \infty$, our model likely falls within this category.

Within our setup, the strength of momentum dissipation (or disorder) represented by k introduces an additional parameter to the system compared to the standard holographic superconductor model (as reviewed in [65]). While the role of k is clear in breaking the translational symmetry explicitly in a complete analysis with backreactions, its direct experimental correspondence remains uncertain. Typically, translational symmetry is indeed broken in real-world materials, but the intensity of this breakage can vary with changes in other parameters. In experiments involving cuprate superconductors, for instance, hole doping p significantly impacts the material properties. Cuprates display superconductivity within a specific doping range, leading to a characteristic dome-shaped phase diagram along the p -axis. It is conjectured that changes in doping levels also lead to variations in k . Another factor that can induce momentum dissipation is the strength of defects, which can be manipulated through processes like irradiation. It's worth noting that translational invariance can also be broken by considering a spatially varying chemical potential $\mu(x)$ [66]. Works such as [67, 68] have introduced charged disorder via a random profile of $\mu(x)$ within the probe limit. The presence of k can be viewed as an analogy to these mechanisms, albeit independent of charge. Establishing a precise connection between k and experimentally controllable parameters would be both intriguing and significant.

It is imperative to acknowledge the constraints imposed by adopting the probe limit in our analysis. Primarily, even when setting $k = 0$, the conductivity in the normal phase does not vanish, contrary to what one might expect. This anomaly arises due to the probe limit itself, which inherently leads to a broken translational symmetry. Secondly, the reliability of our results diminishes significantly at low temperatures, particularly in the O_1 theory where this issue is pronounced. Indeed, we encountered an insurmountable challenge in obtaining solutions for the superconducting phase below the temperature threshold of $T = k/(2\sqrt{2}\pi)$ within the O_1 theory. While the root cause of this mathematical conundrum remains elusive, it is reasonable to speculate that addressing these issues would require incorporating backreactions into the model. In Appendix A, we have numerically verified that the phase boundary calculated under the probe limit does indeed align with the full result when considering a large value of q along with the appropriate scaling factors. While the probe limit methodology introduces these complications, it simultaneously simplifies the model's analysis considerably, making it a practical starting point despite its inherent limitations. Future work, encompassing a more comprehensive treatment of backreactions, is necessary to overcome these constraints and achieve a more accurate depiction of the system's behavior, especially at low temperatures and for the O_1 theory.

The neutral black hole solution provided by Eq. (5) has proven instrumental in our probe limit study of the Gubser-Rocha superconductor model, a pioneering endeavor, to the best of our knowledge. While the AC conductivity calculation with this black hole has been examined in [49], and the same neutral geometry sans k was briefly mentioned in Appendix B of [50], this paper offers the first comprehensive probe limit analysis within this specific model. Expanding upon this groundwork, it would be intriguing to tackle more complex scenarios that are challenging to study in a full back-reaction analysis, such as spatially inhomogeneous solutions [69] or the temporal evolution of the system [70, 71]. The inclusion of a running dilaton can yield distinct outcomes from standard holographic superconductor setups in the SAdS₄ spacetime, although it is essential to remember that the dilatonic black hole represents the genuine ground state only when the temperature satisfies $T < k/(2\sqrt{2}\pi)$.

Moreover, exploring the impact of magnetic fields in our model promises to be equally fascinating. A dyonic black hole geometry in the Gubser-Rocha model serves as the normal phase vacuum, as recently investigated in Ref. [72]. However, in the probe limit, our neutral black hole geometry remains applicable since the Maxwell fields are uncoupled from gravity, as evidenced in analogous

studies within the SAdS₄ context [27, 73]. Here, the effect of an external magnetic field solely permeates the system through the coupled Maxwell-scalar sector under the probe limit conditions. By introducing such a magnetic field, it is anticipated that the phase boundaries and condensates will be altered accordingly. Of particular significance is the role played by the dynamical $U(1)$ gauge field in capturing various magnetic field effects [73–75]. Holographic superconductors featuring dynamical $U(1)$ gauge fields are known to emulate type II superconductors, and the penetration depth computed in their presence constitutes a crucial quantity that can be more directly compared to experimental findings. These areas remain ripe for future research endeavors.

Acknowledgments

We would like to thank Sang-Jin Sin, Matteo Baggioli, Xinmao Yin, Hui Xing, and Di-fan Zhou for their helpful comments. We are grateful to Hyun-Sik Jeong for suggestive comments, especially about the thermodynamic stability of the background black hole geometry. This work is partly supported by NSFC, China (Grant No. 12275166 and No. 12311540141).

Appendix A Checking the correctness of the probe limit

In this section, we compare the T_c - k curve obtained by the probe limit analysis with those obtained for general q . Firstly, we briefly review the charged black hole solutions of our model (1), and its thermodynamic stability. From the full action (1), the equations of motion are obtained as

$$\nabla_\mu \left(e^{\frac{\phi}{\sqrt{3}}} F^{\mu\nu} \right) - iq\Phi^* (\partial^\nu - iqA^\nu) \Phi + iq\Phi (\partial^\nu + iqA^\nu) \Phi^* = 0, \quad (62)$$

$$\nabla^2 \phi - \frac{1}{4\sqrt{3}} e^{\frac{\phi}{\sqrt{3}}} F^2 + 2\sqrt{3} \sinh \left(\frac{\phi}{\sqrt{3}} \right) - B'(\phi) |\Phi|^2 = 0, \quad (63)$$

$$D_\mu D^\mu \Phi - B(\phi) \Phi = 0, \quad \nabla^2 \psi_I = 0. \quad (64)$$

The Einstein's equation is

$$\begin{aligned} R_{\mu\nu} - \frac{1}{2} g_{\mu\nu} \left[R - \frac{1}{4} e^{\frac{\phi}{\sqrt{3}}} F^2 - \frac{1}{2} (\partial\phi)^2 + 6 \cosh \left(\frac{\phi}{\sqrt{3}} \right) - \frac{1}{2} \sum_{I=1}^2 (\partial\psi_I)^2 - |D\Phi|^2 - B(\phi) |\Phi|^2 \right] \\ = \frac{1}{2} e^{\frac{\phi}{\sqrt{3}}} F_{\mu\delta} F_\nu{}^\delta + \frac{1}{2} \partial_\mu \phi \partial_\nu \phi + \frac{1}{2} \sum_{I=1}^2 (\partial_\mu \psi_I \partial_\nu \psi_I) + \frac{1}{2} (D_\mu \Phi D_\nu^* \Phi^* + D_\nu \Phi D_\mu^* \Phi^*). \end{aligned} \quad (65)$$

The normal phase solution is obtained as the following charged dilatonic black hole solution [45]:

$$ds^2 = -f(r)dt + \frac{dr^2}{f(r)} + h(r)(dx^2 + dy^2), \quad (66)$$

with

$$h(r) = r^2 \left(1 - \frac{P}{r} \right)^{1/2}, \quad f(r) = h(r) \left[1 - \frac{k^2}{2r^2} - \frac{r_h^3}{r^3} \left(1 - \frac{k^2}{2r_h^2} \right) \right], \quad (67a)$$

$$\phi(r) = -\frac{\sqrt{3}}{2} \ln \left(1 - \frac{P}{r} \right), \quad \Phi = 0, \quad \psi_I = kx^I, \quad (67b)$$

$$A = \sqrt{3Pr_h \left(1 - \frac{k^2}{2r_h^2} \right)} \left(1 - \frac{r_h}{r} \right) dt, \quad (67c)$$

where r_h is the location of the black hole horizon and P is a physical parameter. Unlike Eq. (5), r_h and k are independent parameters here. Note that this is the same solution as those in Ref. [46], but the coordinate is different. Writing the radial coordinate in [46] as \tilde{r} , we obtain the relation between ours and their conventions as $\tilde{r} + Q = r$, $\tilde{r}_h + Q = r_h$ and $Q = P$. The Hawking temperature and the chemical potential are related to the parameters by

$$T = \frac{1}{8\pi} \frac{6r_h^2 - k^2}{r_h} \sqrt{1 - \frac{P}{r_h}}, \quad \mu = \sqrt{3Pr_h \left(1 - \frac{k^2}{2r_h^2}\right)}. \quad (68)$$

One can see that the neutral limit of Eq. (5) is archived by setting $r_h = k/\sqrt{2}$, whereas $P = 0$ leads Eq. (7). $P/r_h \rightarrow 1$ corresponds to the extremal limit. For the thermodynamic analysis, the grand potential (density) of this solution is given by [44, 51]

$$\Omega(\mu, T; k) = -r_h^3 \left(1 + \frac{1 - P/r_h}{2} \frac{k^2}{r_h^2}\right). \quad (69)$$

The grand potential implicitly depends on μ and T via P and r_h .

On the other hand, the model also admit the following solution: [41]

$$h(r) = r^2, \quad f = r^2 \left[1 - \frac{k^2}{2r^2} + \frac{r_h^2 \mu^2}{4r^4} - \frac{r_h^3}{r^3} \left(1 - \frac{k^2}{2r_h^2} + \frac{\mu^2}{4r_h^2}\right)\right], \quad (70a)$$

$$A = \mu \left(1 - \frac{r_h}{r}\right) dt, \quad \phi = \Phi = 0, \quad \psi_I = kx^I, \quad (70b)$$

where μ, k and r_h are integration constants, which parameterize the family of the solution. μ is directly read as the chemical potential. The temperature is given by

$$T = \frac{r_h}{4\pi} \left(3 - \frac{k^2}{2r_h^2} - \frac{\mu^2}{4r_h^2}\right). \quad (71)$$

One can see $\mu = 0$ leads the neutral solution of Eq. (7). The grand potential of this solution is given by [41]

$$\Omega(\mu, T; k) = -r_h^3 \left(1 + \frac{k^2}{2r_h^2} + \frac{\mu^2}{4r_h^2}\right). \quad (72)$$

The grand potential implicitly depends on T , again.

Let us now consider which solution and parameter range correspond to the ground state of the normal phase. From Eq. (68), there are two distinct parameter regions yielding $T, \mu > 0$ for the dilatonic black hole; i) $0 < P < r_h$ and $0 < k < \sqrt{2}r_h$ ii) $P < 0$ and $\sqrt{2}r_h < k < \sqrt{6}r_h$.⁹ The both choice of the patches cover the entire region of the physical parameter-space like $(k/T, \mu/T)$. On the other hand, $k < \sqrt{6r_h^2 - \mu^2}/2$ is obtained from Eq. (71) for the bald black hole. To determine the ground state, we need to compare the grand potential among these cases. It was investigated in [44], and the answer is that the $P > 0$ patch of the dilatonic black hole is always ground state. Figure 10 shows the competition of the grand potential among these solutions for fixed $\mu/T = 5.0$. Ω_{bald} denotes Eq. (72). $\Omega_{P>0}$ and $\Omega_{P<0}$ denote Eq. (69) in the $P > 0$ and $P < 0$ patches, respectively. The curves exhibit that $\Omega_{\text{bald}} - \Omega_{P<0} < 0$, $\Omega_{P>0} - \Omega_{P<0} < 0$ and $\Omega_{P>0} - \Omega_{P<0} < \Omega_{\text{bald}} - \Omega_{P<0}$. It reads $\Omega_{P>0} < \Omega_{\text{bald}} < \Omega_{P<0}$. Therefore, we conclude that the $P > 0$ patch is the ground state, which is thermodynamically favored [44]. We have checked this behavior of the grand potentials does not change for another choice of μ/T .

Now, we consider the linear perturbation of the charged scalar around the normal phase solution. The form of the equation of motion for the charged scalar is unchanged from (13) in the probe limit

⁹In terms of the original parameter \tilde{r}_h , the ranges of such parameter regions become more complicated.

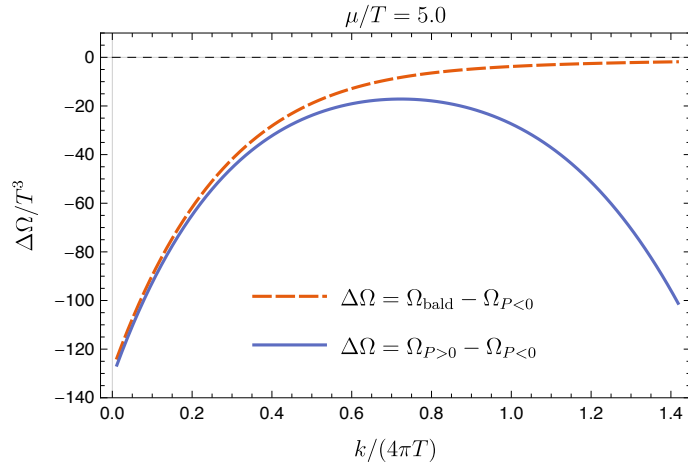


Figure 10: Difference of the grand potentials among the charged black hole solutions. We fix $\mu/T = 5.0$. The result implies $\Omega_{P>0} < \Omega_{\text{bald}} < \Omega_{P<0}$.

analysis. In the backreacted case, the equation can no longer be written in the form of the SL problem. We numerically solve the equation to find T_c (or μ_c). In general, we can obtain multiple eigenvalues and eigenfunctions. The solution with no node is considered as the most relevant solution to the instability.

Figures 11 and 12 show the phase boundaries in the $\frac{T}{q\mu} - \frac{k}{q\mu}$ plane for various q in each theory. The results for $q = \infty$ denote the results obtained by using the neutral solution (5) and (7), i.e., the results in the probe limit. We set $\tau = 0$ here for simplicity. As we have mentioned, there are two patches giving reasonable results satisfying $T > 0$ and $\mu > 0$. Although the $P > 0$ patch is the ground state, we show the results for both patches here. In both patches, we have checked that the corresponding eigenfunctions do not have any node in their radial profile. In Fig. 11, one can see that the result of the $P < 0$ patch agrees with the result in the neutral dilatonic black hole (7) for large q , in the O_1 theory. Meanwhile, the result of the $P > 0$ patch agrees with the result in the neutral bald black hole (7) for large q . Thus, the results of the ground state in the charged case, which is the $P > 0$ patch, correspond to the result of the ground state in the neutral limit. It is consistent. We can also see similar observation from Fig. 12, in the O_2 theory. Depending on the true ground state, the result of the $P > 0$ patches approaches the result in the neutral bald solution above $T = k/(2\sqrt{2}\pi)$, while it approaches the result in the neutral dilatonic solution below $T = k/2(2\sqrt{2}/\pi)$. Note that the $P > 0$ curve for $q = 6$ corresponds to one of the results shown in Ref. [46]. These direct comparisons imply that we need to consider the phase transition of the black hole in the probe limit for obtaining results that agree with the results of the full analysis computed in the true ground state, for large q .

Appendix B Low temperature approximation for the AC conductivity in the SC phase

In this section, we show another approximation of the AC conductivity in the superconducting phase following the method studied in [25]. Unfortunately, however, it does not provide useful results in our model.

In superconducting phase, to study the AC conductivity, we need to solve Eq. (37). Imposing the infalling boundary condition at the horizon, we write

$$A_x(z) = (1 - z)^{\frac{-i\omega}{4\pi T}} G(z) \quad (73)$$

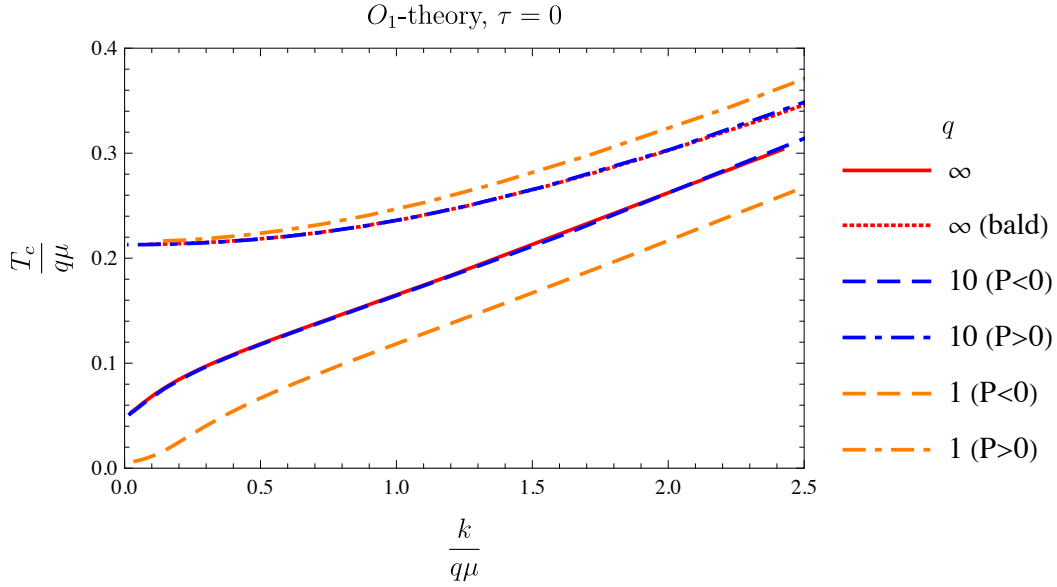


Figure 11: Superconducting phase boundaries of the O_1 theory in the $\frac{T_c}{q\mu}-\frac{k}{q\mu}$ plane for various q . The results for $q = \infty$ denote the results in the probe limit. The dashed/dot-dashed curves corresponds to the negative/positive patches of P . The red dotted curve for $q = \infty$ denotes the result in the bald black hole solution. The $q = 10$ curves almost overlap with the $q = \infty$ curves.

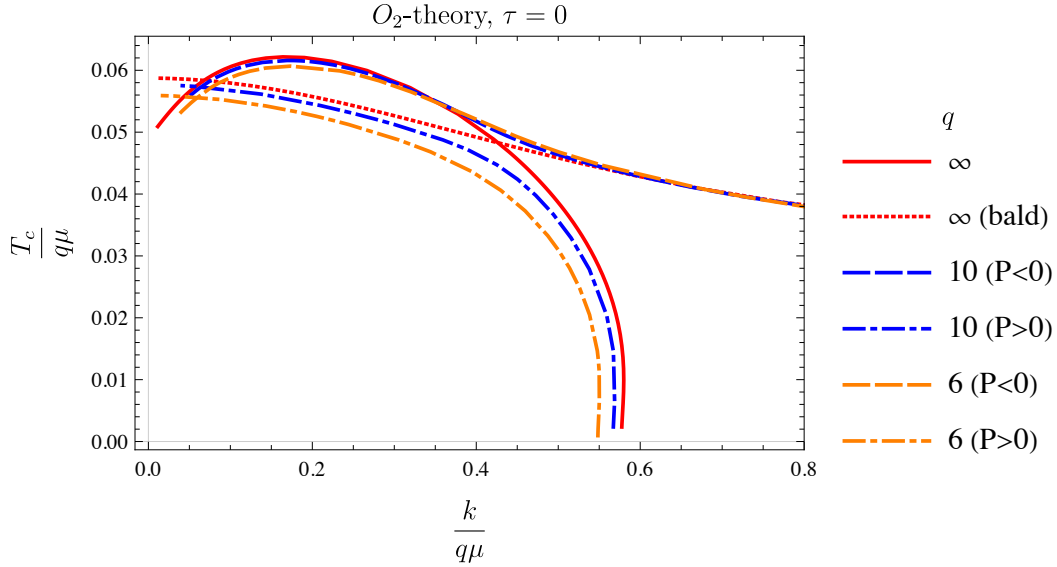


Figure 12: Superconducting phase boundaries of the O_2 theory in the $\frac{T_c}{q\mu}-\frac{k}{q\mu}$ plane for various q . The results for $q = \infty$ denote the results in the probe limit. The dashed/dot-dashed curves corresponds to the negative/positive patches of P .

where $G(z)$ is a regular function at $z = 1$. $G(z)$ can be expanded as

$$G(z) = \alpha_0 + \alpha_1(1 - z) + \alpha_2(1 - z)^2 + \dots \quad (74)$$

Substituting Eq. (73) into Eq. (37), we get

$$G''(z) + \left(\frac{2}{z} + \frac{i\omega}{2\pi T(1-z)} + \frac{f'(z)}{f(z)} + \frac{\phi'(z)}{\sqrt{3}} \right) G'(z) + \frac{1}{48z^4} \left\{ -\frac{3\omega z^3 (4i\pi T(-2+z) + \omega z)}{\pi^2 T^2 (-1+z)^2} + \frac{4}{f(z)^2} \left(12\omega^2 r_h^2 - 24e^{-\frac{\phi(z)}{\sqrt{3}}} q^2 r_h^2 f(z) \Phi(z)^2 - \frac{i\omega z^4 f(z) (3f'(z) + \sqrt{3}f(z)\phi'(z))}{\pi T(-1+z)} \right) \right\} G(z) = 0 \quad (75)$$

The equation involves $\Phi(z)$. We focus on the O_1 theory here.

In order to solve Eq. (75), we utilize the method which develops in [25]. We rewrite the coordinate as $z = \varepsilon\zeta$, and expand the equation for small ε . We choose $\varepsilon = 2\pi T / \langle O_1 \rangle$ to consider the low temperature limit. For small ε , Eq. (75) becomes

$$\frac{\partial^2 G}{\partial \zeta^2} - (1 - \tilde{P}) G + \varepsilon \frac{i\tilde{\omega}}{\sqrt{1 - \tilde{P}}} \frac{\partial G}{\partial \zeta} + \mathcal{O}(\varepsilon^2) = 0, \quad (76)$$

where $\tilde{P} = P/r_h$ and $\tilde{\omega} = \omega/r_h$. We truncate this equation up $\mathcal{O}(\varepsilon^2)$. The general solution is obtained as

$$G = e^{-\frac{i\omega/r_h}{\sqrt{1-P/r_h}}\varepsilon\zeta} \left\{ c_1 e^{-\zeta \sqrt{(1-\frac{P}{r_h}) - \frac{\varepsilon^2}{4} \frac{\omega^2/r_h^2}{1-P/r_h}}} + c_2 e^{\zeta \sqrt{(1-\frac{P}{r_h}) - \frac{\varepsilon^2}{4} \frac{\omega^2/r_h^2}{1-P/r_h}}} \right\}. \quad (77)$$

In the original z coordinate, we write

$$G(z) \approx e^{-\frac{i\omega/r_h}{\sqrt{1-P/r_h}}z} \left\{ c_1 e^{+\frac{z\varepsilon^{-1}}{\sqrt{1-P/r_h}}} + c_2 e^{-\frac{z\varepsilon^{-1}}{\sqrt{1-P/r_h}}} \right\}. \quad (78)$$

Here, we have dropped the higher ε terms in the exponential terms. Recalled $A_x(z) = (1-z)^{\frac{-i\omega}{4\pi T}} G(z)$, the conductivity is obtained as

$$\sigma(\omega) \approx i \frac{\langle O_1 \rangle}{\omega} \frac{1 - c_1/c_2}{1 + c_1/c_2}. \quad (79)$$

Now, we consider fixing the ratio c_1/c_2 by using the equation at $z = 1$:

$$G'(1) \left(1 - \frac{i\tilde{\omega}}{\sqrt{1 - \tilde{P}}} \right) + \frac{1}{16} G(1) \left(16q^2 \Phi(1)^2 - 4\tilde{\omega}^2 \frac{1 - 2\tilde{P}}{(1 - \tilde{P})^2} - \frac{4i\tilde{\omega}}{\sqrt{1 - \tilde{P}}} \right) = 0. \quad (80)$$

Note that the equation involves unknown parameter $\Phi(1)$. We assume that the scalar profile can be approximated by $\Phi(z) = \frac{\langle O_1 \rangle}{r_h \sqrt{2}} z$. Then, $\Phi(1)$ is given by $\Phi(1) = \langle O_1 \rangle / (r_h \sqrt{2})$. Using Eqs. (73), (78) and (80), the ratio c_1/c_2 becomes ($\omega \rightarrow 0$)

$$\frac{c_1}{c_2} \approx e^{2\frac{\sqrt{1-\tilde{P}}}{\varepsilon}} \left[1 + \frac{2\tilde{O}_1^2(1 - \tilde{P})^2 - i\tilde{\omega} \left(3(1 - \tilde{P})^{3/2} - i\tilde{\omega}(3 - 4\tilde{P}) \right)}{2(1 - \tilde{P})^2(-i\tilde{\omega} + \sqrt{1 - \tilde{P}})} \varepsilon \right], \quad (81)$$

where $\tilde{O}_1 = \langle O_1 \rangle / r_h$. We have dropped the higher ε terms again. Plugging this to (79), the conductivity is written as

$$\sigma(\omega) \approx \frac{i\tilde{O}_1}{\tilde{\omega}} \left[1 - 2e^{-2\tilde{O}_1} \left(1 + \frac{2\tilde{O}_1^2(1-\tilde{P})^2 - i\tilde{\omega}(3(1-\tilde{P})^{3/2} - i\tilde{\omega}(3-4\tilde{P}))}{2\tilde{O}_1(1-\tilde{P})^{3/2}(\sqrt{1-\tilde{P}} - i\tilde{\omega})} \right)^{-1} \right]. \quad (82)$$

The low frequency expansion is obtained

$$\sigma(\omega) \approx \frac{i\tilde{O}_1}{\tilde{\omega}} \left[1 - \frac{2}{1+\tilde{O}_1} e^{-2\tilde{O}_1} + i\tilde{\omega} \frac{2\tilde{O}_1^2 - 3}{\tilde{O}_1(\tilde{O}_1 + 1)^2 \sqrt{1-\tilde{P}}} e^{-2\tilde{O}_1} + \mathcal{O}(\tilde{\omega}) \right]. \quad (83)$$

The leading coefficient corresponds to the superfluid density which can be read

$$n_s \approx \langle O_1 \rangle - \frac{2\langle O_1 \rangle}{\langle O_1 \rangle + r_h} e^{-2\langle O_1 \rangle / r_h}. \quad (84)$$

However, the approximation becomes better when $\langle O_1 \rangle \gg r_h$, so the contribution from the second term is very small. Neglecting the second term, we obtain the same result for n_s read from Eq. (60).

References

- [1] J. Bardeen, L. N. Cooper, and J. R. Schrieffer, *Theory of Superconductivity*, Phys. Rev. **108**, 1175–1204 (1957).
- [2] J. G. Bednorz and K. A. Müller, *Possible high T_c superconductivity in the Ba-La-Cu-O system*, Z. Physik B - Condensed Matter **64**, 189–193 (1986).
- [3] M. K. Wu et al., *Superconductivity at 93 K in a new mixed-phase Y-Ba-Cu-O compound system at ambient pressure*, Phys. Rev. Lett. **58**, 908 (1987).
- [4] H. Maeda et al., *A New High- T_c Oxide Superconductor without a Rare Earth Element*, Jpn. J. Appl. Phys. **27** L209 (1988).
- [5] Z. Z. Sheng and A. M. Hermann, *Bulk superconductivity at 120 K in the Tl-Ca/Ba-Cu-O system*, Nature **332**, 138–139 (1988).
- [6] J. J. Hamlin et al., *Superconductivity in single crystals of LaFePO*, J. Phys.: Condens. Matter **20**, 365220 (2008). [arXiv:0806.1265 [cond-mat.supr-con]]
- [7] Y. Kamihara et al., *Iron-based layered superconductor La[O_{1-x}F_x]FeAs ($x = 0.05-0.12$) with $T_c = 26$ K*, J. Am. Chem. Soc. **130**, 11, 3296–3297 (2008).
- [8] X. H. Chen, T. Wu, G. Wu, R. H. Liu, H. Chen and D. F. Fang, *Superconductivity at 43 K in SmFeAsO_{1-x}F_x*, Nature **453**, 761–762, (2008).
- [9] H. H. Wen et al., *Superconductivity at 25 K in hole-doped (La_{1-x}Sr_x)OFeAs*, Europhys. Lett. **82** (2008) 17009 (2008). [arXiv:0803.3021 [cond-mat.supr-con]]
- [10] M. Mondal et al., *Phase Fluctuations in a Strongly Disordered s-Wave NbN Superconductor Close to the Metal-Insulator Transition*, Phys. Rev. Lett. **106**, 047001 (2011).
- [11] S. Mandal et al., *Destruction of superconductivity through phase fluctuations in ultrathin a-MoGe films*, Phys. Rev. B **102**, 060501 (2020). [arXiv:2003.12398 [cond-mat.supr-con]]

- [12] S. S. Mandal and T. V. Ramakrishnan, *Microscopic free energy functional of superconductive amplitude and phase: Superfluid density in disordered superconductors*, Phys. Rev. B **102**, 024514 (2020).
- [13] L. Hetel, T. R. Lemberger and M. Randeria, *Quantum critical behaviour in the superfluid density of strongly underdoped ultrathin copper oxide films*, Nature Phys. **3**, 700-702 (2007).
- [14] D. Deepwell et al., *Microwave conductivity and superfluid density in strongly overdoped $Tl_2Ba_2CuO_{6+\delta}$* , Phys. Rev. B, **88**, 214509 (2013).
- [15] I. Božović, X. He, J. Wu and A. T. Bollinger, *Dependence of the critical temperature in overdoped copper oxides on superfluid density*, Nature **536**, 309-311 (2016).
- [16] J. M. Maldacena, *The Large N limit of superconformal field theories and supergravity*, Adv. Theor. Math. Phys. **2**, 231-252 (1998). [arXiv:hep-th/9711200 [hep-th]]
- [17] E. Witten, *Anti-de Sitter space and holography*, Adv. Theor. Math. Phys. **2**, 253-291 (1998). [arXiv:hep-th/9802150 [hep-th]]
- [18] S. S. Gubser, I. R. Klebanov and A. M. Polyakov, *Gauge theory correlators from noncritical string theory*, Phys. Lett. B **428**, 105-114 (1998). [arXiv:hep-th/9802109 [hep-th]]
- [19] J. Zaanen, Y. Liu, Y-W. Sun, K. Schalm, *Holographic Duality in Condensed Matter Physics*, (Cambridge, Cambridge University Press, 2016).
- [20] M. Ammon and J. Erdmenger, *Gauge/Gravity Duality: Foundations and Applications*. (Cambridge, Cambridge University Press, 2015).
- [21] M. Baggioli, *Applied Holography: A Practical Mini-Course*, (Springer, 2019). [arXiv:1908.02667 [hep-th]]
- [22] R. G. Cai, L. Li, L. F. Li and R. Q. Yang, *Introduction to Holographic Superconductor Models*, Sci. China Phys. Mech. Astron. **58**, no.6, 060401 (2015) [arXiv:1502.00437 [hep-th]]
- [23] S. A. Hartnoll, C. P. Herzog, G. T. Horowitz, *Building an AdS/CFT superconductor*, Phys. Rev. Lett. **101**, 031601 (2008). [arXiv:0803.3295 [hep-th]]
- [24] S. A. Hartnoll, C. P. Herzog and G. T. Horowitz, *Holographic Superconductors*, JHEP **12**, 015 (2008). [arXiv:0810.1563 [hep-th]]
- [25] G. Siopsis and J. Therrien, *Analytic Calculation of Properties of Holographic Superconductors*, JHEP **05**, 013 (2010). [arXiv:1003.4275 [hep-th]]
- [26] G. T. Horowitz and M. M. Roberts, *Zero Temperature Limit of Holographic Superconductors*, JHEP **11**, 015 (2009). [arXiv:0908.3677 [hep-th]]
- [27] X. H. Ge, B. Wang, S. F. Wu and G. H. Yang, *Analytical study on holographic superconductors in external magnetic field*, JHEP **08**, 108 (2010). [arXiv:1002.4901 [hep-th]]
- [28] S. Franco, A. Garcia-Garcia and D. Rodriguez-Gomez, *A General class of holographic superconductors*, JHEP **04**, 092 (2010). [arXiv:0906.1214 [hep-th]]
- [29] R. G. Cai, Z. Y. Nie and H. Q. Zhang, *Holographic p-wave superconductors from Gauss-Bonnet gravity*, Phys. Rev. D **82**, 066007 (2010). [arXiv:1007.3321 [hep-th]]

- [30] D. Roychowdhury, *Effect of external magnetic field on holographic superconductors in presence of nonlinear corrections*, Phys. Rev. D **86**, 106009 (2012). [arXiv:1211.0904 [hep-th]]
- [31] S. Gangopadhyay, *Holographic superconductors in Born-Infeld electrodynamics and external magnetic field*, Mod. Phys. Lett. A **29**, 1450088 (2014). [arXiv:1311.4416 [hep-th]]
- [32] J. Erdmenger, X. H. Ge and D. W. Pang, *Striped phases in the holographic insulator/superconductor transition*, JHEP **11**, 027 (2013). [arXiv:1307.4609 [hep-th]]
- [33] X. H. Ge, S. J. Sin and S. F. Wu, *Universality of DC Electrical Conductivity from Holography*, Phys. Lett. B **767**, 63-68 (2017). [arXiv:1512.01917 [hep-th]]
- [34] A. Sheykhi, H. R. Salahi and A. Montakhab, *Analytical and Numerical Study of Gauss-Bonnet Holographic Superconductors with Power-Maxwell Field*, JHEP **04**, 058 (2016). [arXiv:1603.00075 [gr-qc]]
- [35] X. Qiao, L. OuYang, D. Wang, Q. Pan and J. Jing, *Holographic superconductors in 4D Einstein-Gauss-Bonnet gravity*, JHEP **12**, 192 (2020). [arXiv:2005.01007 [hep-th]]
- [36] Z. Zhao, W. Cai and S. Ishigaki, *Doped Holographic Superconductors in Gubser-Rocha model*, (2023). [arXiv:2309.14851 [hep-th]]
- [37] J. Yuan et al. *Scaling of the strange-metal scattering in unconventional superconductors*. Nature **602**, 431–436 (2022).
- [38] X. Y. Jiang et al. *Interplay between superconductivity and the strange-metal state in FeSe*. Nat. Phys. **19**, 365–371 (2023).
- [39] P. W. Phillips, N. E. Hussey and P. Abbamonte, *Stranger than metals*, Science **377**, no.6602, eabh4273 (2022). [arXiv:2205.12979 [cond-mat.str-el]]
- [40] S. S. Gubser and F. D. Rocha, *Peculiar properties of a charged dilatonic black hole in AdS₅*, Phys. Rev. D **81**, 046001 (2010). [arXiv:0911.2898 [hep-th]]
- [41] T. Andrade and B. Withers, *A simple holographic model of momentum relaxation*, JHEP **05**, 101 (2014). [arXiv:1311.5157 [hep-th]]
- [42] B. Goutéraux, *Charge transport in holography with momentum dissipation*, JHEP **04**, 181 (2014). [arXiv:1401.5436 [hep-th]]
- [43] Z. Zhou, Y. Ling and J. P. Wu, *Holographic incoherent transport in Einstein-Maxwell-dilaton Gravity*, Phys. Rev. D **94**, no.10, 106015 (2016). [arXiv:1512.01434 [hep-th]]
- [44] K. Y. Kim and C. Niu, *Diffusion and Butterfly Velocity at Finite Density*, JHEP **06**, 030 (2017). [arXiv:1704.00947 [hep-th]]
- [45] H. S. Jeong, K. Y. Kim and C. Niu, *Linear- T resistivity at high temperature*, JHEP **10**, 191 (2018). [arXiv:1806.07739 [hep-th]]
- [46] H. S. Jeong and K. Y. Kim, *Homes' law in holographic superconductor with linear- T resistivity*, JHEP **03**, 060 (2022). [arXiv:2112.01153 [hep-th]]
- [47] R. A. Davison, K. Schalm and J. Zaanen, *Holographic duality and the resistivity of strange metals*, Phys. Rev. B **89**, no.24, 245116 (2014). [arXiv:1311.2451 [hep-th]]

- [48] H. S. Jeong, *Quantum Chaos and Pole-Skipping in Semi-Locally Critical IR*, [arXiv:2309.13412 [hep-th]].
- [49] J. Ren and W. Zheng, *Analytic AC conductivities from holography*, Phys. Rev. D **105**, no.6, 066013 (2022). [arXiv:2109.07481 [hep-th]]
- [50] J. Ren and H. Xie, *Holographic superconductors at zero density*, Phys. Rev. D **107**, no.10, 106004 (2023). [arXiv:2206.03498 [hep-th]]
- [51] M. M. Caldarelli, A. Christodoulou, I. Papadimitriou and K. Skenderis, *Phases of planar AdS black holes with axionic charge*, JHEP **04**, 001 (2017). [arXiv:1612.07214 [hep-th]]
- [52] S. Cremonini and L. Li, *Criteria For Superfluid Instabilities of Geometries with Hyperscaling Violation*, JHEP **11**, 137 (2016). [arXiv:1606.02745 [hep-th]]
- [53] E. Witten, *Multitrace operators, boundary conditions, and AdS/CFT correspondence*, (2001). [arXiv:hep-th/0112258 [hep-th]]
- [54] T. Andrade, S. A. Gentle, *Relaxed superconductors*, JHEP **06** 140 (2015) [arXiv:1412.6521[hep-th]]
- [55] D. T. Son and A. O. Starinets, *Minkowski space correlators in AdS / CFT correspondence: Recipe and applications*, JHEP **09**, 042 (2002). [arXiv:hep-th/0205051 [hep-th]]
- [56] C. P. Herzog, P. Kovtun, S. Sachdev and D. T. Son, *Quantum critical transport, duality, and M-theory*, Phys. Rev. D **75**, 085020 (2007). [arXiv:hep-th/0701036 [hep-th]]
- [57] S. A. Hartnoll, A. Lucas and S. Sachdev, *Holographic quantum matter*, (Cambridge, The MIT Press, 2018) [arXiv:1612.07324 [hep-th]]
- [58] Y. J. Uemura et al., *Universal Correlations between T_c and $\frac{n_s}{m^*}$ (Carrier Density over Effective Mass) in High- T_c Cuprate Superconductors*, Phys. Rev. Lett. **62**, 2317 (1989).
- [59] Y. J. Uemura et al., *Basic Similarities among Cuprate, Bismuthate, Organic, Chevrel-Phase, and Heavy-Fermion Superconductors Shown by Penetration-Depth Measurements*, Phys. Rev. Lett. **68**, 2712 (1991).
- [60] C. C. Homes et al., *Universal scaling relation in high-temperature superconductors*, Nature **430**, 539 (2004). [arXiv:cond-mat/0404216 [cond-mat.supr-con]]
- [61] C. C. Homes et al., *Scaling of the superfluid density in high-temperature superconductors*, Phys. Rev. **B 72**, 134517 (2005). [arXiv:cond-mat/0410719 [cond-mat.supr-con]]
- [62] S. V. Dordevic and C. C. Homes, *Superfluid density in overdoped cuprates: Thin films versus bulk samples*, Phys. Rev. B **105**, 214514 (2022).
- [63] B. Goutéraux and E. Mefford, *Normal charge densities in quantum critical superfluids*, Phys. Rev. Lett. **124**, no.16, 161604 (2020). [arXiv:1912.08849 [hep-th]].
- [64] B. Goutéraux and E. Mefford, *Non-vanishing zero-temperature normal density in holographic superfluids*, JHEP **11**, 091 (2020). [arXiv:2008.02289 [hep-th]].
- [65] M. Baggioli, K. Y. Kim, L. Li and W. J. Li, *Holographic Axion Model: a simple gravitational tool for quantum matter*, Sci. China Phys. Mech. Astron. **64**, no.7, 270001 (2021) [arXiv:2101.01892 [hep-th]].

- [66] G. T. Horowitz, J. E. Santos and D. Tong, *Optical Conductivity with Holographic Lattices*, JHEP **07**, 168 (2012) [arXiv:1204.0519 [hep-th]].
- [67] D. Arean, A. Farahi, L. A. Pando Zayas, I. S. Landea and A. Scardicchio, *Holographic superconductor with disorder*, Phys. Rev. D **89**, no.10, 106003 (2014). [arXiv:1308.1920 [hep-th]].
- [68] D. Arean, L. A. Pando Zayas, I. S. Landea and A. Scardicchio, *Holographic disorder driven superconductor-metal transition*, Phys. Rev. D **94**, no.10, 106003 (2016). [arXiv:1507.02280 [hep-th]].
- [69] V. Keranen, E. Keski-Vakkuri, S. Nowling and K. P. Yogendran, *Dark Solitons in Holographic Superfluids*, Phys. Rev. D **80**, 121901 (2009). [arXiv:0906.5217 [hep-th]]
- [70] H. B. Zeng, Y. Tian, Z. Fan and C. M. Chen, *Nonlinear Conductivity of a Holographic Superconductor Under Constant Electric Field*, Phys. Rev. D **95**, no.4, 046014 (2017). [arXiv:1611.06798 [hep-th]]
- [71] P. Yang, M. Baggioli, Z. Cai, Y. Tian and H. Zhang, *Holographic Dissipative Spacetime Super-solids*, Phys. Rev. Lett. **131**, no.22, 221601 (2023). [arXiv:2304.02534 [hep-th]]
- [72] X. H. Ge and Z. Xu, *Thermo-electric transport of dyonic Gubser-Rocha black holes*, JHEP **03**, 069 (2024). [arXiv:2310.12067 [hep-th]]
- [73] O. Domenech, M. Montull, A. Pomarol, A. Salvio and P. J. Silva, *Emergent Gauge Fields in Holographic Superconductors*, JHEP **08**, 033 (2010). [arXiv:1005.1776 [hep-th]]
- [74] A. Salvio, *Holographic Superfluids and Superconductors in Dilaton-Gravity*, JHEP **09**, 134 (2012). [arXiv:1207.3800 [hep-th]].
- [75] A. Salvio, *Transitions in Dilaton Holography with Global or Local Symmetries*, JHEP **03**, 136 (2013). [arXiv:1302.4898 [hep-th]].